The structural anatomy of the Pyrenees examined through EMAG2v2 magnetic data.

África Gamisel-Muzás[1,2], Ruth Soto[2], Conxi Ayala[3], Tania Mochales[2], Félix M. Rubio[2], Pilar Clariana[2], Carmen Rey-Moral[2], Juliana Martín-León[2].

5   [1] Instituto Andaluz de Ciencias de la Tierra, IACT-CSIC, 18100 Armilla, Granada. a.gamisel@csic.es.
[2] Instituto Geológico y Minero de España (IGME), CSIC, 28003, 28760, 50059. r.soto@igme.es, t.mochales@igme.es, fm.rubio@igme.es, p.clariana@igme.es, c.rey@igme.es, j.martin@igme.es.
[3] Geosciences Barcelona (GEO3BCN), CSIC, Lluís Solé i Sabarís s/n, 08028 Barcelona. cayala@geo3bcn.csic.es

10   *Correspondence to:* A. Gamisel-Muzás (a.gamisel@csic.es)

Abstract. The major goal of this work is to provide an insight into the structural anatomy of the Pyrenees based on the magnetic data from the Earth Magnetic Anomaly Grid 2-arc-minute resolution (EMAG2v2). We focused on providing qualitative and semi-quantitative evidence on the magnetic signature of the Pyrenees Mountain

15   Range domains and structures. The integration of reduced to the pole and processed maps, as well as the Bouguer anomaly map with geological data, has proved to be significantly useful in order to shed light on the main anomaly sources. Considering their magnetic response and texture, several anomalies can be linked to buried geological bodies or changes in the magnetic character of the basement. We have estimated their source bodies depth through Euler and power spectrum calculations.

20   We have identified eight magnetic zones with different features and interpreted them in terms of the geological and structural setting of the area. The result is an overall interpretation of the Pyrenees main magnetic domains.

[Margin annotation: In the abstract rather than saying what was done. In abstract, provide key results: what are the source depths in different locations, what type of geologic sources in these eight magnetic zones and specific characteristics of magnetic anomalies associated in these zones]

1. Introduction

The characterization of the Earth's crustal structure and composition through geophysical data has represented a

25   significant challenge in Geoscience over the last century. Among various geophysical exploration methods, aeromagnetic surveying has emerged during the last century, initially performed during the World War II (Nabighian et al., 2005). Magnetic surveying has proven to be highly effective to investigate the Earth's crust at different scales, from mapping basement structures to constraining the extent of saline diapirs. The aeromagnetic data surveying allows to cover large areas in a short period of time without being invasive (e.g. Vine and

30   Matthews, 1963; Vine, 1966; Gibson and Millegan, 1998; Langel and Hinze, 1998; Golynsky, 2002; Purucker and Whaler, 2007; Maus et al., 2009). The processing of the acquired data allows generating magnetic anomaly maps that provide valuable information concerning both continental terrains and Earth's oceanic floors (e.g. Müller et al., 2008). In particular, large-scale magnetic anomaly maps are of great interest for analyzing major lineaments and structural trends (e.g. Maus et al., 2009) that can be used to improve geological mapping (e. g.

35   Ayala et al., 2000, García-Lobón et al., 2007).

Concerning the Pyrenees, numerous geological and geophysical studies have been conducted to infer their crustal structure at depth (e.g. ECORS-Pyrenees Team, 1988; Casas et al., 1997; Chevrot et al., 2014, 2018). However, their overall study based on magnetic data has received less attention (Zeyen and Banda, 1989; Zeyen et al., 1991). In this study we utilize data from the Earth Magnetic Anomaly Grid (EMAG2v2) (Maus et al., 2009), to interpret

40   the magnetic patterns related to the geological structure of the Pyrenees. This study highlights the effectiveness

[Margin annotations: "geosciences" (over "represented"); "remained?"; "continental assemblies (give references for both examples)"]

of magnetic anomaly maps in interpreting the structural characteristics of the Pyrenees and gives an overall view of its magnetic complexity.

2. Data and methodology.

The magnetic data used in this analysis came from EMAG2v2 (2009) version instead of the EMAG2v3 (Meyer

45 et al., 2017) due to the lack of data of the latter in the study area. The homogenized grid of the EMAG2v2 incorporates the aeromagnetic survey data from France (Institut du Physique du Globe de Paris – Bureau de Recherches Géologiques et Minières, 1960) and Spain (Socías et al., 1991 - Instituto Geográfico Nacional, 1986-1987) as well as international satellite and ship data. It consists of a homogenized grid displaying the magnetic anomalies at 4000 meters above the geoid with a spatial resolution of 2-arc-min (equivalent, at this latitude, to

50 ~3700 meters) (Maus et al. 2009). The magnetic anomaly map of the studied area has been integrated into a digital database to compare it with the main Pyrenean structures, gravimetric anomalies and the main outcrops of intrusive and volcanic rocks.

To enhance the interpretation of the magnetic signal of the Pyrenees, derivative maps and estimated calculations of the location and depth of the magnetic sources have been generated from the total magnetic field. This enables

55 us to improve and complete the correlation between geophysical and geological information. These calculations were made through the Oasis Montaj© software by Seequent.

2.1. Reduction to pole (RTP).

This magnetic transformation aims to eliminate the inherent asymmetry present in total magnetic field anomalies, locating the anomalies above the causative bodies. This is achieved by converting the observed anomaly to the

60 equivalent anomaly measured at the North Magnetic Pole (Baranov 1957; Baranov and Naudy, 1964). This transformation assumes that the remanent magnetization is negligible compared to the induced magnetization. The advantage of this transformation is that the resulting map is easier to correlate with the surface geology and other geophysical data, like gravity, which helps with the interpretation.

2.2. Magnetic derivatives.

65 The magnetic derivatives have been proved effective to locate the diverse anomaly sources since they accentuate the outline of their boundaries, and sometimes even estimate their depth, the inclination and susceptibility contrast between rocks (e.g. Verduzco et al., 2004). In this study, we have applied these calculations on the reduced to the pole magnetic field.

The vertical derivative (VDR_Z) usually highlights the shallowest anomaly sources because enhances the high

70 wavenumber component of the spectrum and exposes positive values above the sources. The horizontal derivative (HDR_X and HDR_Y) outlines the anomaly source bodies since it produces a phase transformation and enhances the higher frequencies (Fanton et al., 2014). The direction of the attributes to highlight plays a crucial role in the latter since it exposes the directional variation of the magnetic field with regard to the magnetic causative bodies, providing a distinctive anomaly texture (Hayatudeen et al., 2021). The horizontal derivative in X (N90ºE)

75 direction will enhance N-S discontinuities and the Y (N180ºE) direction will enhance E-W discontinuities. Additionally, directional derivatives in N110ºE and N200ºE would enhance the structures following the main Pyrenean directions. As a combination of both vertical and horizontal derivatives of the magnetic anomalies, the analytic signal shows symmetric maximum values above the anomaly sources (Ansari and Alamdar, 2009).

Initially described by Miller and Singh (1994) as an innovative method to distinguish the anomalies as well as

80 their edges and peaks, the tilt derivative (TDR) combines the horizontal and vertical derivatives, later refined by

2

Verduzco et al., (2004). Consequently, the tilt angle answers to both horizontal and vertical derivatives on magnetization, so weak magnetic bodies are weighted the same as strongly magnetized ones (Blakely et al., 2016). The vertical derivative positive values peak above the source has zero value along its edge and turns negative outside of the source. The horizontal gradient is positive along the edges and is zero above the source (Miller and

85   Singh, 1994). The tilt angle derivative is zero on the edge of the anomalies. It is well suited to locate anomalies despite their depth due to the equalization of the amplitudes of short and long wavelength anomalies (Lahti and Tuomo, 2010). However, the horizontal derivative of the tilt derivative (TDR_THDR), invariant of geomagnetic inclination, is capable of providing sharp and well-defined peaks the source edges. Despite being accurate defining shallow sources it may be ambiguous about deep bodies (Ma and Li, 2012).

90   **2.3. Euler deconvolution.**

Euler deconvolution is a technique to estimate the depth of the anomalous sources (Thomson, 1982; Reid et al., 1990) based on the x, y and z derivatives of the data and a parameter called structural index (SI) (Cooper, 2008). The SI is related to the geometry of the anomaly sources (Cooper, 2008; Reid et al., 1990). Each Euler solution is calculated according to the data within a window (WS) (Reid et al., 1990) that is recommended to be at least half

95   of the size of the anomaly to compute (FitzGerald et al., 2004). SI=0 is usually adequate to define contacts or steps of the causative bodies, whereas S=0.5 and SI=1 is rather suitable to determine dike or sills.

2.4.   **Power spectrum.**

The spectral analysis of the magnetic data provides information about the depth of the magnetic sources attending to magnetic contrasts (Maus and Dimri, 1995; Peredo et al., 2021). The spectrum pattern is a good approach to

100   estimate the depth of the causative bodies. When plotting the natural logarithm of the spectrum against the radial frequency (or the wavenumber), the different linear segments of the spectrum showed in the graph can be associated with different geological discontinuities. The depth (z) is determined by the slope of each segment (m) according to the formula $z= m/4\pi$ (Spector and Grant, 1970; Peredo et al., 2021).

3.   **Geological setting of the study area.**

105   This study focuses on the magnetic characterization of the Pyrenees, bordered by the Bay of Biscay to the West and the Gulf of Lion to the East. The study area comprises 110184 km^2 within the ETRS89 UTM31 coordinates, with the NW corner located at, 81985, 4860782, and the SE corner located at, 539073, 4578415 (coordinates in meters, Fig.1). In addition, some areas at the eastern termination of the mountain range will also be described due to the occurrence of important magnetic anomalies like Olot, La Garrotxa Volcanic field (e.g. Zeyen and Banda,

110   1988), and the western part of the Gulf of Lion passive margin (e.g. Canva et al., 2020) (see Fig. 1).
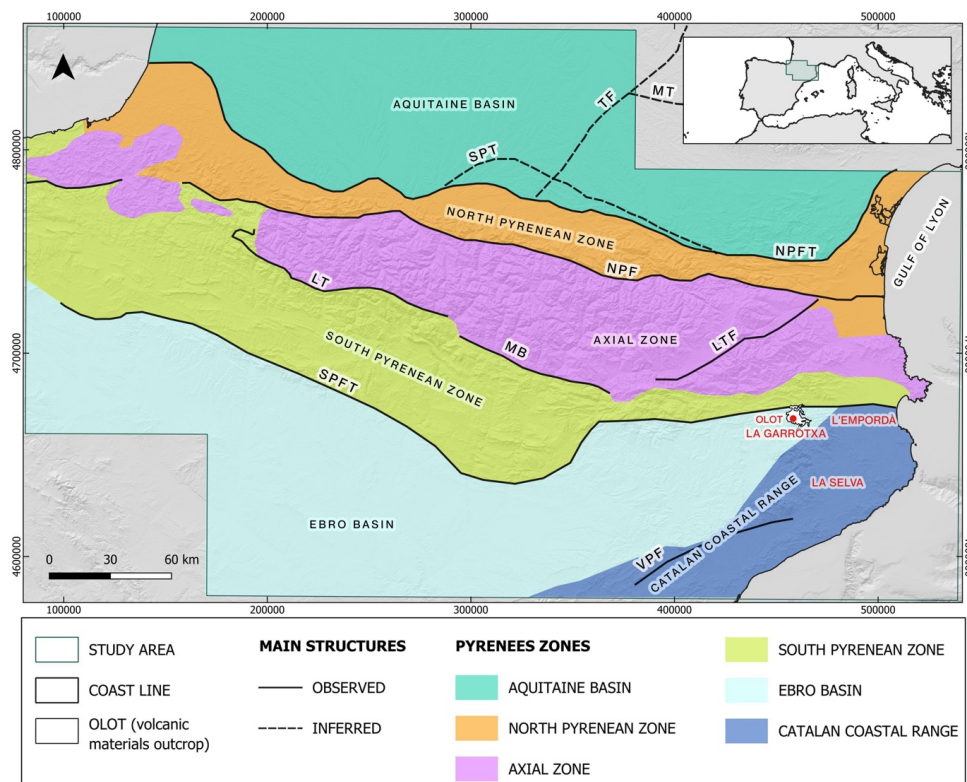
Fig.1. Geological major units differentiated in the Pyrenees and surrounding areas. Relief map of the study area. Data obtained from the IGN (Instituto Geográfico Nacional, Spain), GEOSERVICE (France) and EMODNET (European Marine Observation and Data Network, Offshore). NPFT: North Pyrenean Frontal Thrust, NPF: North Pyrenean Fault, LT: Lakora Thrust, MB: Morreres Back Thrust, LTF: La Tet Fault, SPT: Sub-Pyrenean Thrust, MT: Mazamet Thrust, TF: Tolouse Fault, SPFT: South Pyrenean Frontal Thrust, VPF: Valles-Penedes Fault. UTM coordinates in m, Zone 31N, ETRS89 datum.

The Pyrenees represent a WNW-ESE double vergence mountain range with a dominant southward vergence resulted from the convergence between the Iberian and European plates (e.g. Muñoz, 1992). It developed as an asymmetric chain from Late Cretaceous to the Early Miocene (e.g. Muñoz, 1992) (Fig.2. A). Deformation along the convergent plates boundaries was accommodated by the underthrusting of the Iberian lithosphere underneath Europe and the thrusting and stacking of the upper crust (e.g. Choukroune and ECORS team, 1989; Roest and Srivastava, 1991; Rosenbaum et al., 2002). The general structure, stratigraphy and geodynamics of the Pyrenees have been extensively studied during the last five decades (e.g. Séguret, 1972; Garrido-Megías, 1973; Muñoz, 1992; Barnolas et al., 1996; Ford et al., 2022). In parallel, many geophysical studies have been carried out to infer the structure at depth of the Pyrenees, mainly based in seismic, gravimetric and magnetotelluric methods (e.g. ECORS-Pyrenees Team, 1988; Casas et al., 1997; Ledo et al., 2000; Chevrot et al., 2014, 2018; Wang et al., 2016; Campanyà et al., 2011).

The formation of the Pyrenees involved a complex geodynamic evolution, including the reactivation and/or inversion of previous Variscan and Mesozoic structures (e.g., Bond and Mclay, 1995; Poblet, 1991; Muñoz, 1992; Clerc and Lagabrielle, 2012, 2014; Ledo et al., 2000; Wher et al., 2018; Le Maire et al., 2021). The Variscan

Orogeny took place during the Carboniferous (e.g. Zwart, 1986; García-Sansegundo, 1996; García-Sansegundo et al., 2011; Casas et al., 2019) while different extensional stages occurred from the Permian to Cretaceous,

135   associated with the opening of the North Atlantic and Bay of Biscay (e.g., Roest and Srivastava, 1991; Ziegler, 1988).

The early stages of Atlantic rifting resulted in the emplacement of subvolcanic tholeiitic dolerites derived from a subcontinental lithospheric mantle, which are now found as isolated outcrops within the Upper Triassic evaporites in the Pyrenees and other regions of Iberia (e.g., Beziat, 1983; Alibert, 1985). The Mesozoic extension culminated

140   in the Pyrenees with the formation of a hyperextended margin during the Albian-Cenomanian, characterized by an extreme crustal thinning and subcontinental lithospheric mantle exhumation within the Northern Pyrenees (e.g. Clerc and Lagabrielle, 2014; Jammes et al., 2009; Lagabrielle et al., 2010, Pedrera et al., 2017).
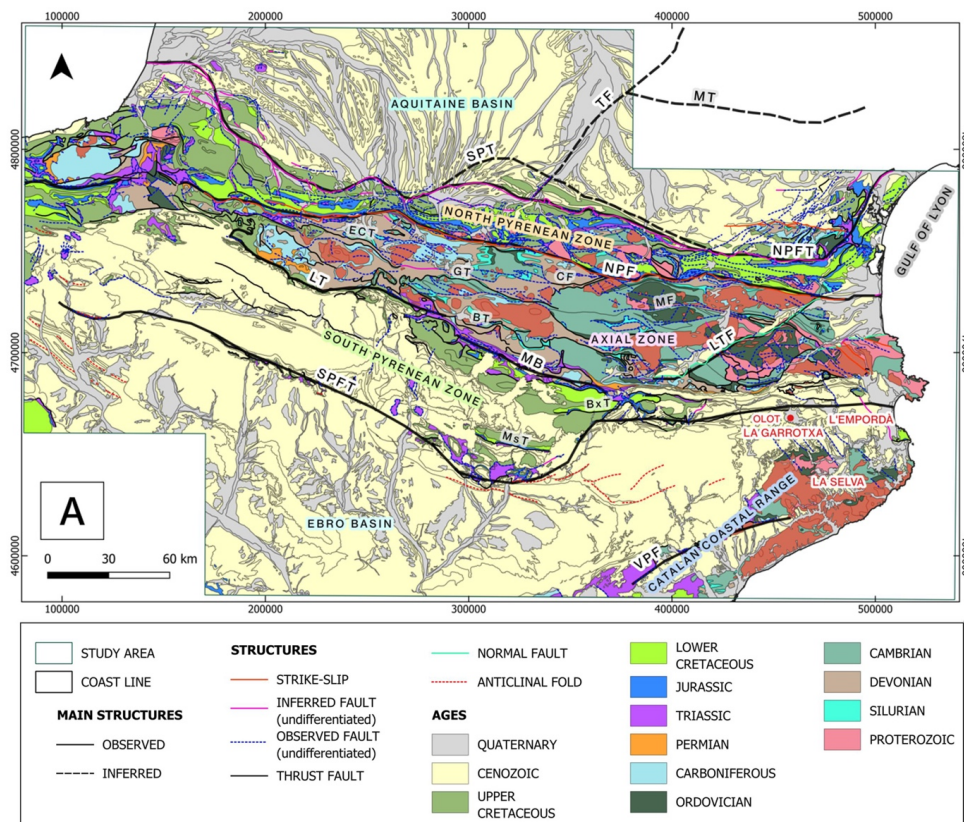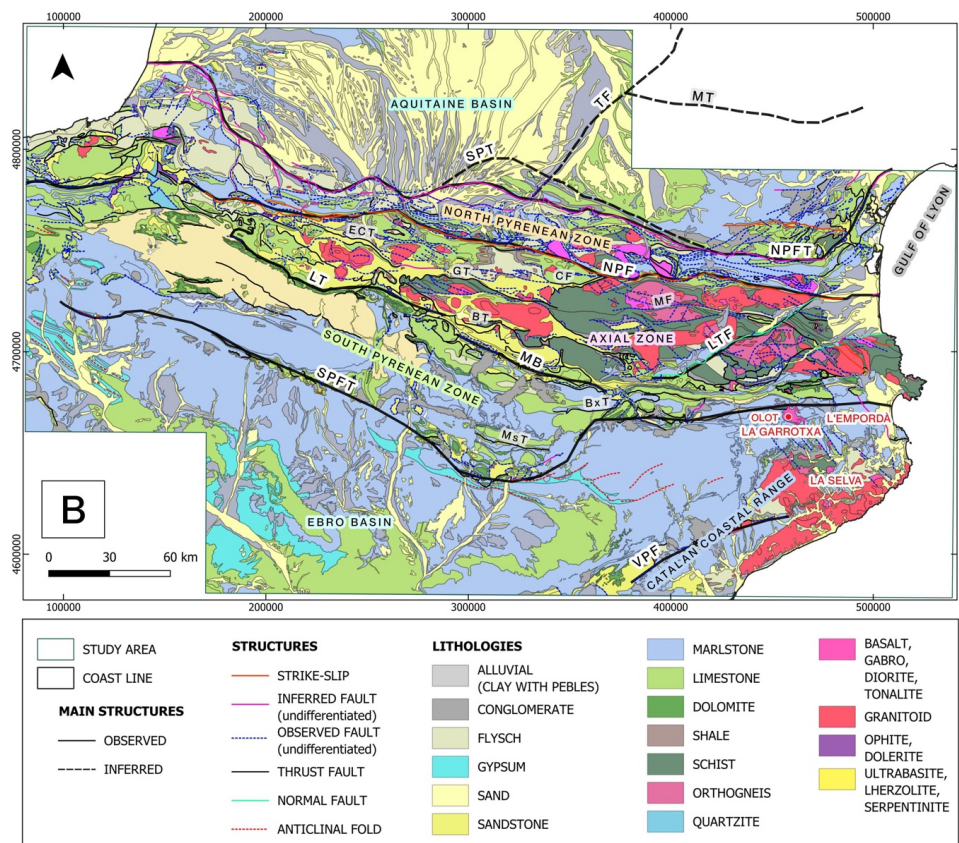
Chronostratigraphic ?

145 **Fig.2. (A) Chronological and structural map (Modified from BRGM-IGME, 2009) (B) Lithological and structural map (Modified from BRGM-IGME, 2009) of the Pyrenees study area. NPFT: North Pyrenean Frontal Thrust, NPF: North Pyrenean Fault, ECT: Eaux-Chaudes Thrust, GT: Gavarnie Thrust, CF: Couflens Fault, MF: Merens Fault, BT: Bono thrust, BxT: Boixols Thrust, MsT: Montsec Thrust, SMT: Sierra Marginales Thrust, LT: Lakora Thrust, MB: Morreres Back Thrust, LTF: La Tet Fault, SPT: Sub-Pyrenean Thrust, MT: Mazamet Thrust, TF: Tolouse Fault,**
150 **SPFT: South Pyrenean Frontal Thrust, VPF: Valles-Penedes Fault. UTM coordinates in m, Zone 31N, ETRS89 datum.**

Geological data of the study (age of units, structure and lithology, (Fig.2. A and B) were obtained from the cartography base map of the IGME-BRGM (2009) through the Geological Survey of Spain (IGME-CSIC) website link: http://info.igme.es/cartografiadigital.

155 **3.1. Pyrenean main tectonic units.**

From North to South, five main tectonic units can be distinguished in the Pyrenees (Barnolas and Pujalte, 2004 and references therein) (Fig.1); the Aquitaine basin (AB), the North Pyrenean Zone (NPZ), the Axial Zone (AZ), the South Pyrenean Zone (SPZ), and the Ebro basin (EB).

The Aquitaine basin (Fig.2. A and B) represents the northern foreland basin developed on the overriding European

160 plate. It has been extensively explored over the last 60 years (e.g. Biteau et al., 2006; Serrano et al., 2006). Its mid-Eocene to Miocene sedimentary fill can be attributed to a foreland subsidence directly linked to the growth of the Pyrenees (e.g. Biteau et al., 2006; Rougier et al., 2016). Geophysical data, like seismic profiles (eg Rougier et al., 2016), have revealed the existence of highly deformed Paleozoic basement rocks at depth and Mesozoic

sub-basins related to an important rift system highly variable along-strike (e.g. Canérot et al., 2005). The Aquitaine basin is mainly deformed at depth between the North Pyrenean Frontal thrust (NPFT) and the Sub-Pyrenean thrust (SPT).

The North Pyrenean Zone is characterized by inverted thick sequences of syn-rift to postrift Mesozoic rocks (e.g. Souquet et al. 1977; Déramond et al., 1988). This zone represents a relatively narrow fold-and-thrust belt, measuring between 25 to 35 kilometers, which has developed along the southern boundary of the European (upper) plate between the North Pyrenean Fault (NPF) and North Pyrenean Frontal thrust (NPFT) (Fig. 2. A and B). Regional high-temperature low pressure (HT-LP) metamorphism and about 40 outcrops of sub-continental peridotites are hosted in the Northern Pyrenees related to the Early Cretaceous hyper-extension and mantle exhumation (e.g. Jammes et al. 2009, 2010; Clerc et al. 2012, Vauchez et al. 2012).

The Axial Zone (Fig. 2. A and B) is located at the core of the alpine chain and comprises an antiformal stack of south-vergent basement thrust sheets. It mainly consists metasedimentary Paleozoic rocks deformed and metamorphosed previously during the Variscan Orogeny, along with variscan granitoids (e.g. Barnolas et al., 1996; Casas et al. 2019). The Axial Zone elevation varies along its strike and exhibits a direct correlation with the depth of the European basement top (e.g. Soto et al., 2006) indicating that the control of the crustal deep configuration of the Pyrenees lays on their structural architecture (e.g. Beaumont et al., 2000; Jammes et al., 2009; Saspiturry et al., 2019; Muñoz, 2019).

The South Pyrenean Zone constitutes a south-verging thin-skinned fold-and-thrust belt detached from the basement along the Middle-Upper Triassic evaporites (e.g. Séguret, 1972; Muñoz, 1992). It is characterized by a Mesozoic succession with an along-strike thickness variation and a thick syn-orogenic Cenozoic sequence (e.g. Séguret, 1972; Garrido-Megías, 1973; Cámara and Klimowitz, 1985; Muñoz, 1992; Soto et al., 2002) (Fig.2. A and B).

Finally, the Ebro basin (Fig. 2. A and B) represents the southern foreland basin of the Pyrenees and encompasses a continuous sequence up to 5500 meters of latest Eocene, Oligocene and Miocene continental sediments (e.g. Alonso-Zarza et al., 2002). Its autochtonous sediments are deformed by several folds and thrusts detached along the Eocene evaporites close to the South Pyrenean Frontal thrust.

4. Data analysis and results.
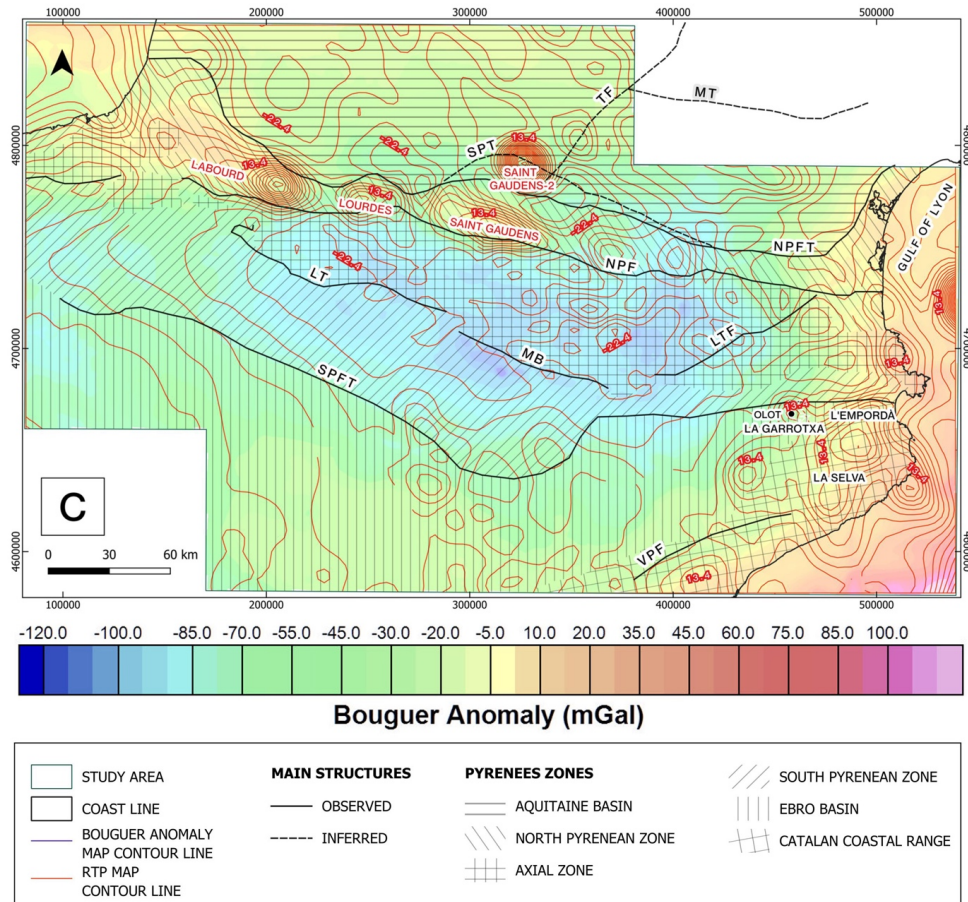
4.1. Reduction to the pole (RTP).

The reduced to the pole magnetic field was calculated according to the declination and inclination parameters corresponding to the average date of data acquisition 1973/06/15.

Determined by the lithologies, the resulting map displays a highly defined and located anomalies above the source bodies (Fig.3.A). Magnetic anomalies values range between -50.2 to 83.24 nT, while the mean value is -5.79 nT. It is noticeable the overlaying of the magnetic anomaly maxima above the Bouguer anomaly maxima (Pedrera et al., 2017) (Fig.3.B and C).

200
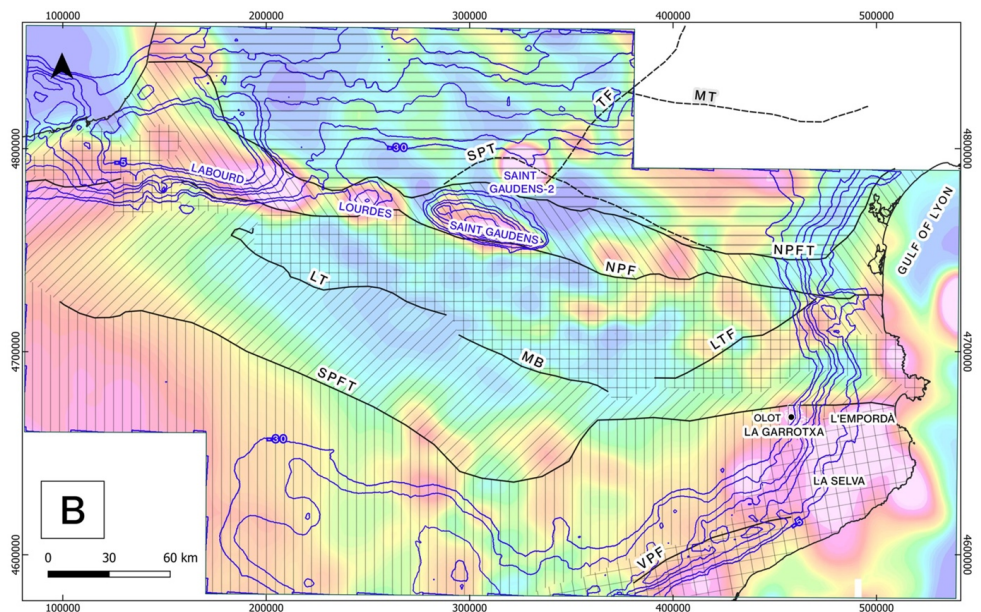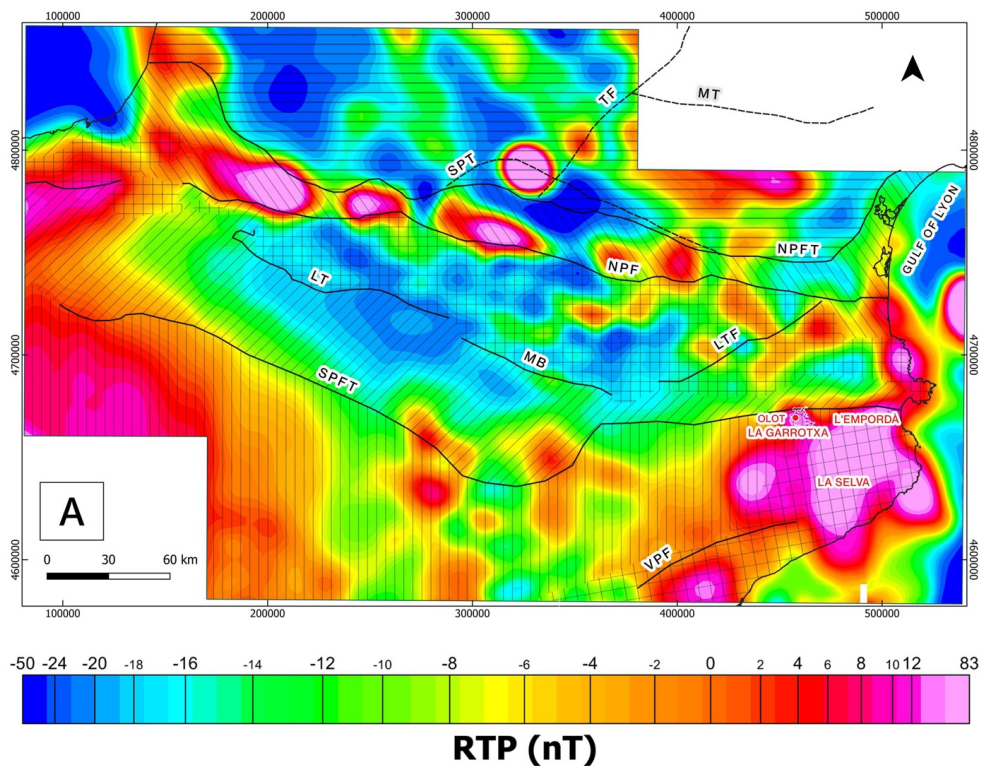
Fig.3. (A) Reduced to the pole (RTP) magnetic map of the study area. (B) RTP map with the Bouguer anomaly contour lines on top. (C) Bouguer anomaly map (Modified from Pedrera et al., 2017) with the RTP contour lines on top. Main structures and Pyrenean zones distinguished by diverse texture patterns are also represented. MT: Mazamet Thrust, TF: Tolouse Fault, SPT: Sub-Pyrenean Thrust, NPFT: North Pyrenean Frontal Thrust, NPF: North Pyrenean Fault, LTF: La tet Fault, MB: Morreres Back Thrust, LT: Lakora Thrust, SPFT: South Pyrenean Frontal Thrust, VPF: Valles-Penedes Fault. UTM coordinates in m, Zone 31N, ETRS89 datum.

On the RTP map (Fig.3.A), wavelength values range from 7 to 125 kilometers. The Pyrenean anomalies can be grouped into magnetic zones that roughly coincide with the main Pyrenean structures.

In the North Pyrenean Zone (Fig. 1, 2. B and 3.A and B), next to the NPFT, the high intensity, short to intermediate wavelength anomalies can be associated with the outcrops of lherzolites, granulites and ophites.

The Axial Zone and South Pyrenean Zone (Fig. 1 and 3. A and B) are characterized by an elongated medium to long wavelength minimum with some short wavelength high amplitude positive and negative anomalies on top. These anomalies could be related to the basement geometry and the accumulation of Triassic evaporites. Given that these anomalies have a NNW-SSE direction, they can also be related to Axial Zone structures. In the South Pyrenean Zone is worth noting the so called Lérida anomaly, a medium wavelength high that could be originated by a basement high within the Ebro Basin (Zeyen and Banda, 1988).

220   Towards the NE, next to the Catalan coast, there is a zone characterized by several maxima that correlates to outcrops of the Olot basaltic volcanic rocks of La Garrotxa and the Volcanic Field of L'Empordà and La Selva. Since these magnetic anomalies are larger than the outcrops of volcanic rocks, this could point to a wider volcanic area than previously thought, with the anomalies also originated by buried volcanic rocks. In the Catalan Coastal Range (CCR), the relative maxima are related with outcrops of Paleozoic basement. Towards its northern

225   termination, their anomalies are masked by the magnetic signature of the La Garrotxa Volcanic Field (Olot).

4.2. Magnetic derivatives.

Since it focuses on shallower sources, the vertical derivative (VDR_Z) map (Fig.4.A) delimits quite well near surface anomalous bodies. Three different magnetic texture zones are distinguished: a set of NNW-SSE lineaments to the north of the Axial Zone; a zone with relatively intermediate anomalies to the Ebro Basin western

230   side; NE-SW lineaments towards the eastern side of the EB, the Catalan Coastal Range and L'Empordà, La Selva and La Garrotxa Volcanic Field.

The horizontal derivative in X (HDR_X) map (Fig.4.B) displays predominantly N-S oriented lineaments along the North Pyrenean Zone, the Axial Zone and the Catalan Coastal Range. These zones also exhibit a strong ESE-WNW component in the horizontal derivative in Y (HDR_Y) map (Fig.4.C), whereas, L'Empordà, La Selva and

235   La Garrotxa Volcanic Field present a more chaotic magnetic pattern.

Horizontal derivatives in N110ºE direction (HDR_110) (Fig.4.D) and N200ºE direction (HDR_200) (Fig.4.E), which are the Pyrenean and its perpendicular main directions, enhance structures in those directions such as La Tet Fault or the Morreres Back Thrust, respectively. HDR_110 seems to be more defined over the Axial Zone and North Pyrenean Zone, and exceptionally eastwards, towards Olot. HDR_200 outlines the southern border of the

240   Axial Zone almost perfectly but has a rather less concordant texture around the other structures.

The analytic signal (AS) (Fig.4.F) shows two different texture zones: the NW-SE half, characterized by rounded shapes above the main anomalies along the North Pyrenean Zone, the Volcanic Field (La Empordà, La Selva, La Garrotxa) and the Gulf of Lyon; the Axial Zone, the South Pyrenean Zone and the Ebro Basin with a diffuse and uneven texture.

245   Lineaments in the tilt derivative (TDR) map (Fig.4.G) appear to be outlining most of the main anomaly bodies that generate the magnetic anomalies on the RTP map (Fig.3.A). The intricate morphology of the North Pyrenean Zone, the Volcanic Field and the Catalan Coastal Range anomaly sources are very well defined. It is worth noting that from the southern border of the Axial Zone northwards (Axial Zone, North Pyrenean Zone, Aquitaine Basin) it displays a NW-SE texture with a N110ºE approximate direction, while a N-S orientation pattern prevail to the

250   south of that boundary (South Pyrenean Zone, Ebro Basin), being Olot (La Garrotxa) the eastern end of both textures. Its horizontal derivative (TDR_THDR) (Fig.4.H) enhances the edges of the anomaly source bodies, exceptionally along the Central Pyrenees.
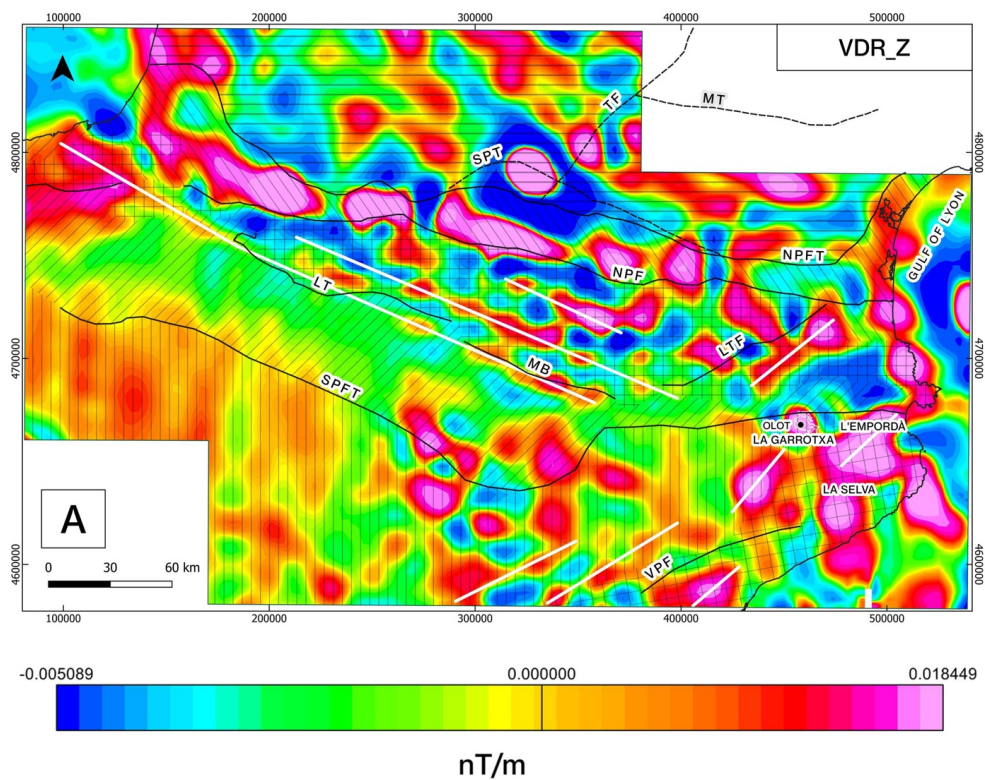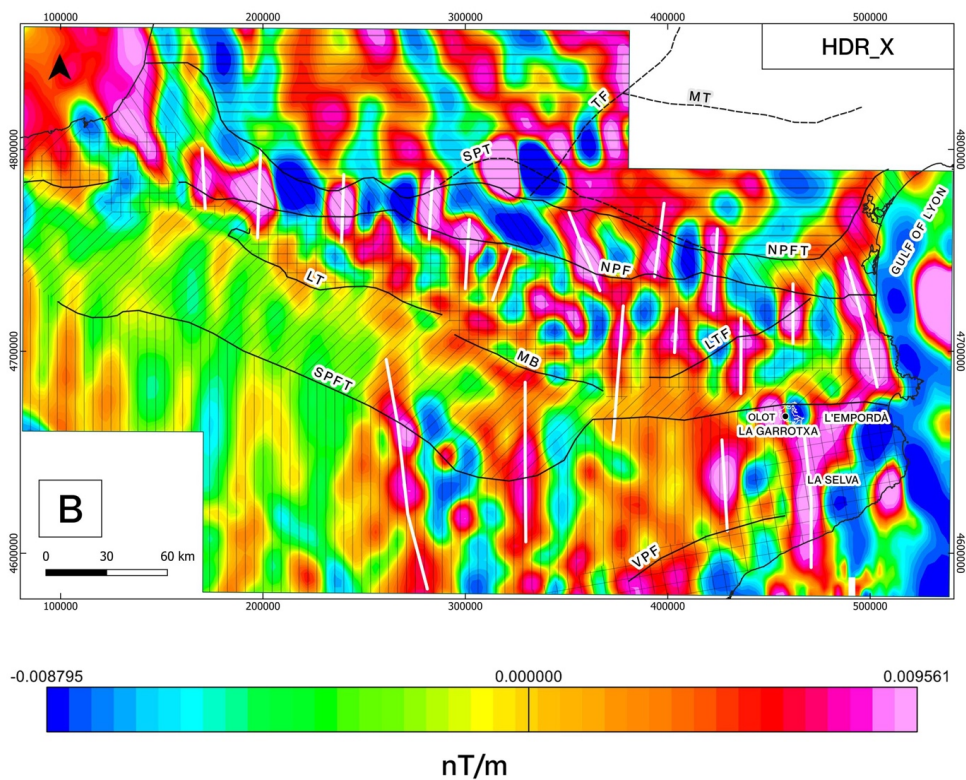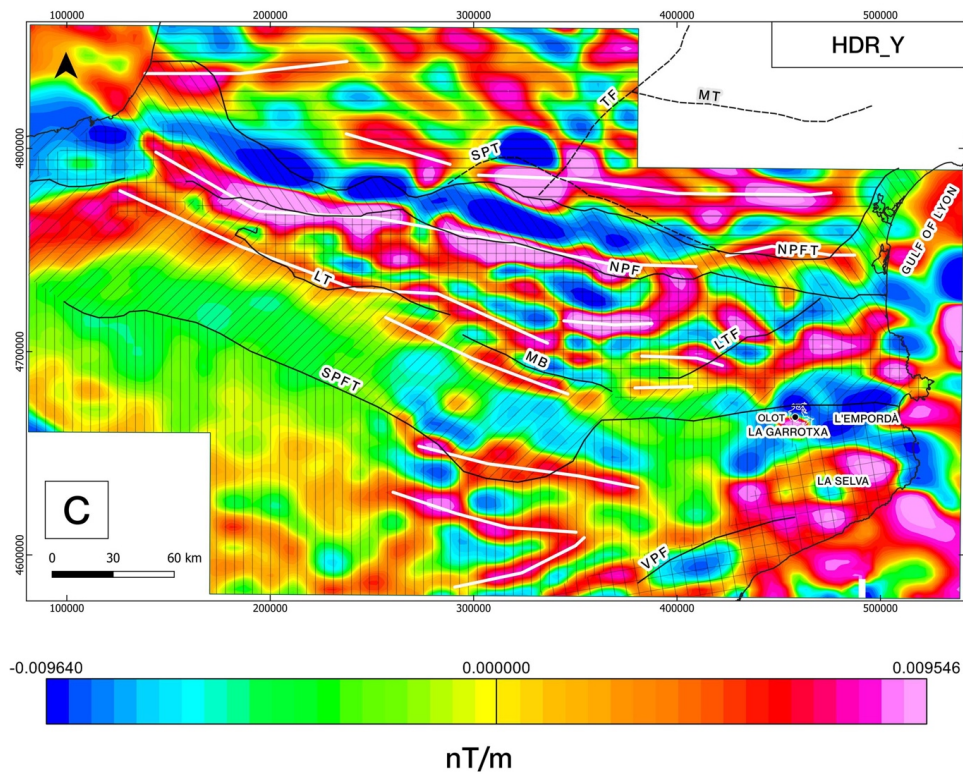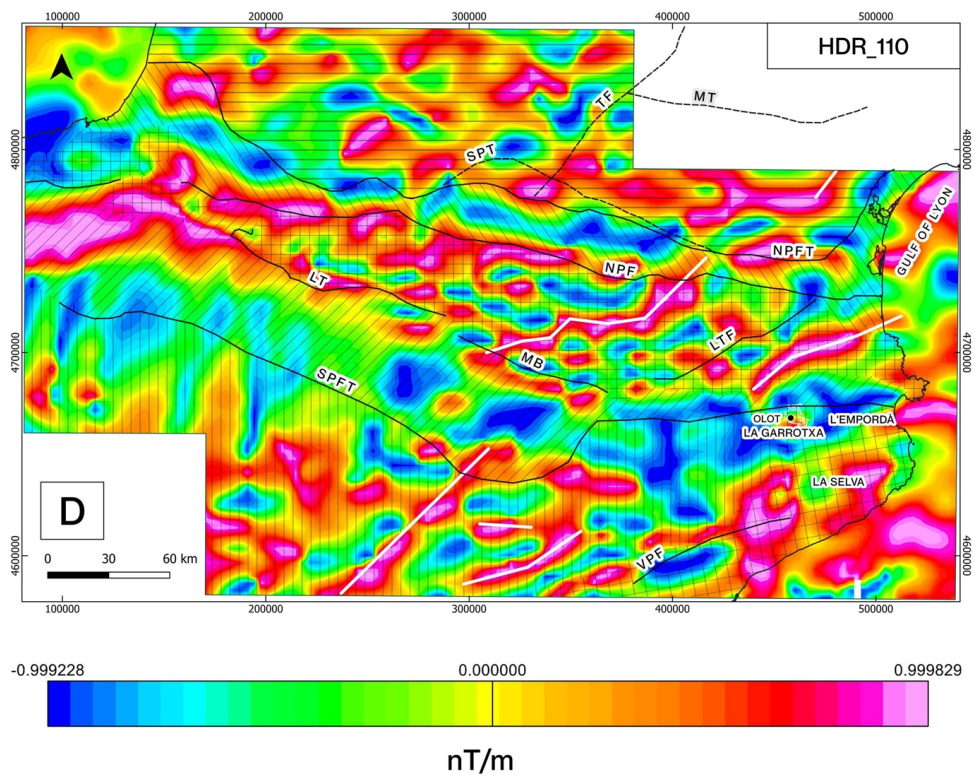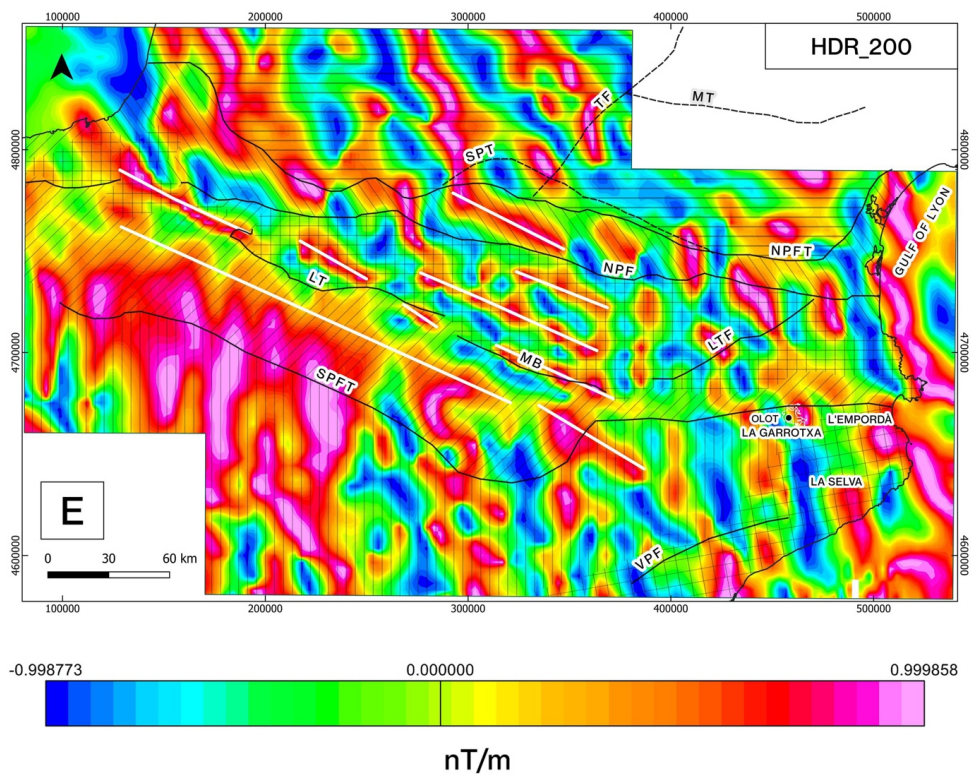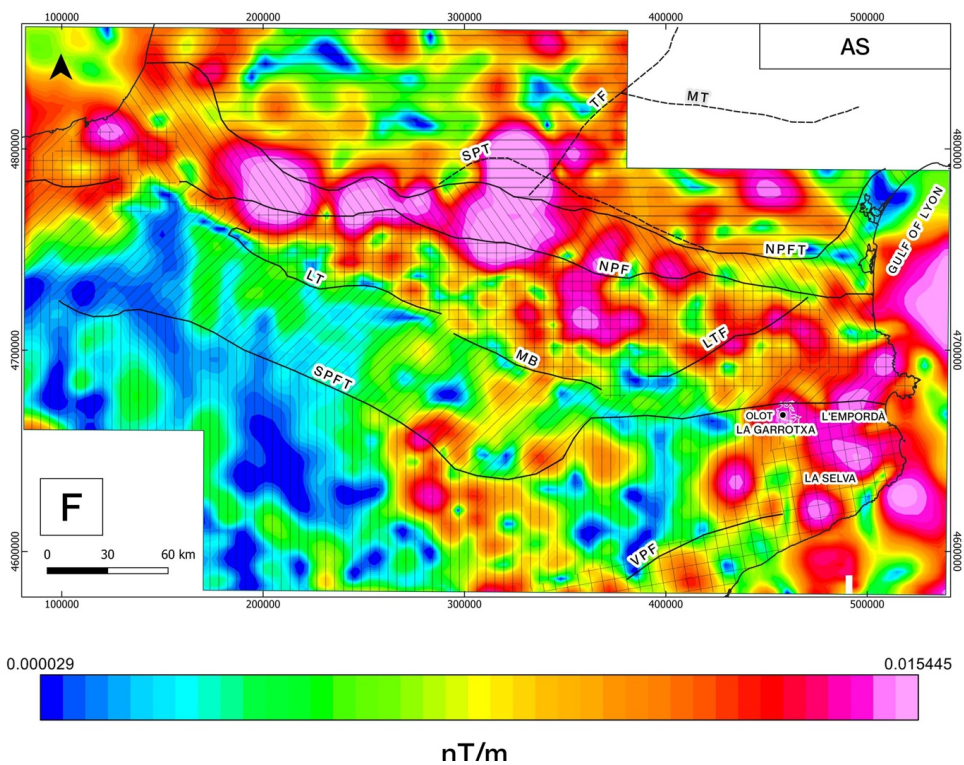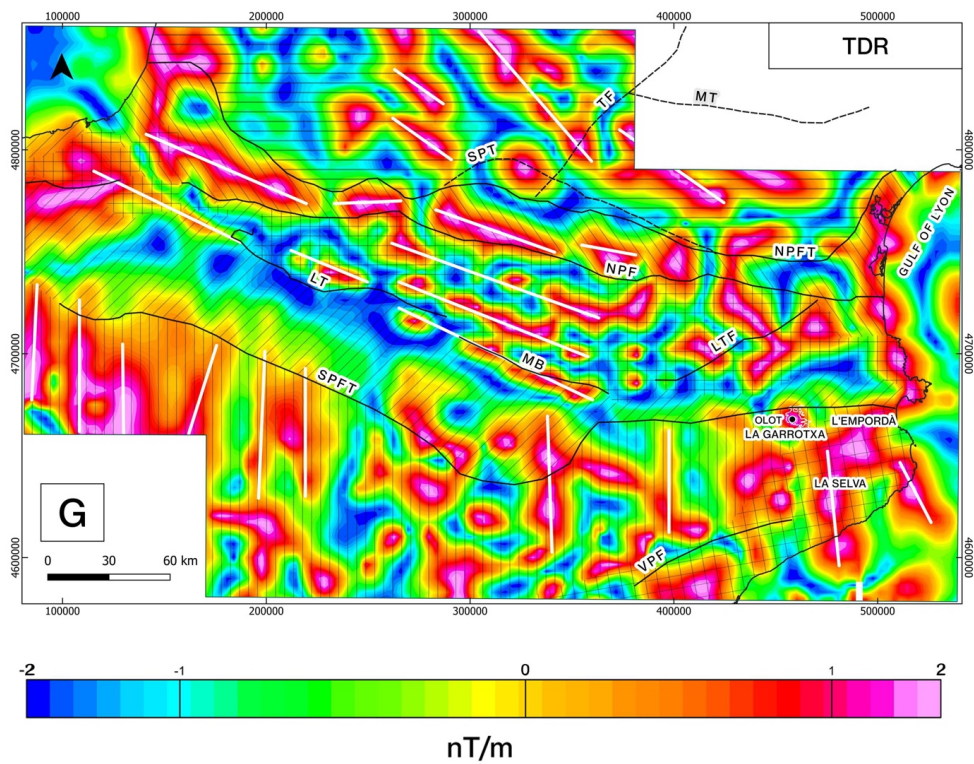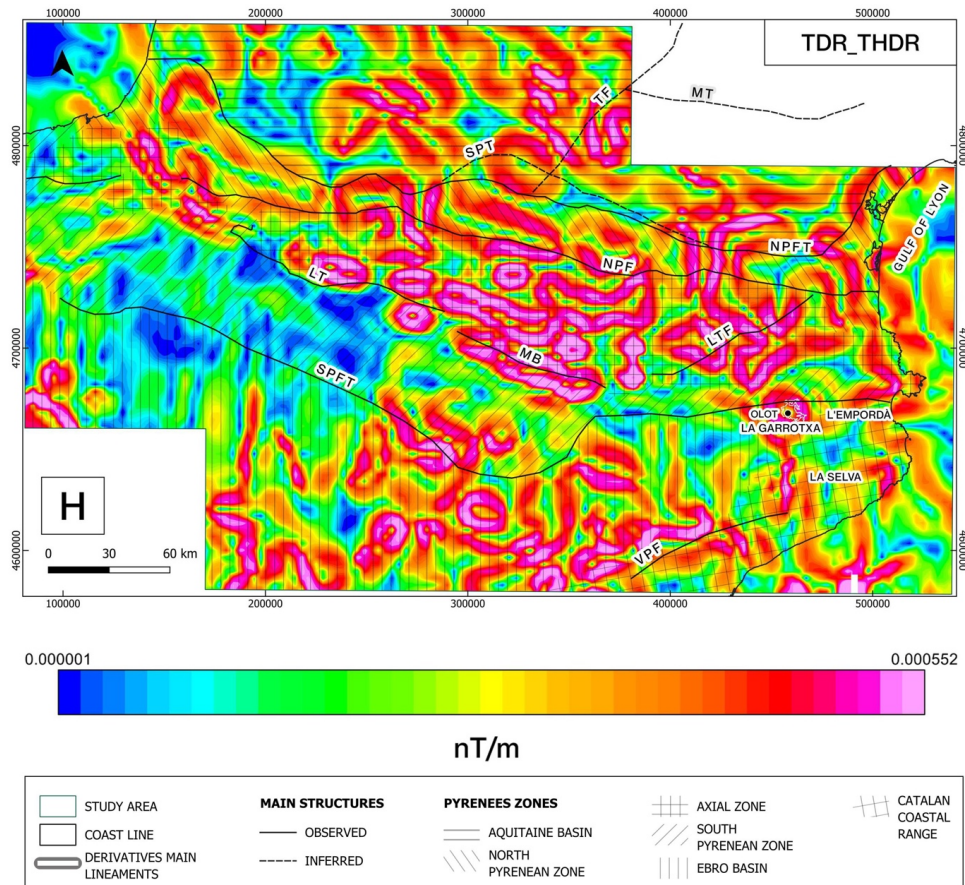
Fig.4. (A) Vertical derivative map (VDR_Z). (B) Horizontal derivative in X map (HDR_X). (C) Horizontal derivative in Y map (HDR_Y). (D) Horizontal derivative in N110ºE map (HDR_110). (E) Horizontal derivative in N200ºE map (HDR_200). (F) Analytic Signal map (AS). (G) Tilt derivative map (TDR). (H) Horizontal derivative of the tilt derivative map (TDR_THDR). In addition, the main lineaments of each derivative and main structures of the study area are also represented. The main Pyrenean zones are differentiated by diverse texture patterns. MT: Mazamet Thrust, TF: Tolouse Fault, SPT: Sub-Pyrenean Thrust, NPFT: North Pyrenean Frontal Thrust, NPF: North Pyrenean Fault, LTF: La tet Fault, MB: Morreres Back Thrust, LT: Lakora Thrust, SPFT: South Pyrenean Frontal Thrust, VPF: Valles-Penedes Fault. UTM coordinates in m, Zone 31N, ETRS89 datum.

4.3. Euler deconvolution.

In order to constrain the depth estimation of the magnetic source bodies, we have used the Euler deconvolution calculation. As indicated in the methodology, we have chosen the parameters SI=0 (contacts/steps) with a window of 5 km and SI=1 (sills/dykes) with a window of 10 km. Each window size was selected to ensure the adjusted record of the whole extension of the target bodies.

For the contacts/steps solutions (SI=0, WS=5) (Fig.5.A) the depth estimation reaches up to 5 km to the north of the North Pyrenean Fault in different clusters, surrounding some of the RTP high positive anomalies, usually near the outcrops of lherzolites and granulites. The deepest solutions (From 3 km to more than 20 km) are located in the western sector of the South Pyernean Zone and the Volcanic Field, while shallower solutions (From 0.1 km to 5 km) are found along the Ebro Basin and the Catalan Coastal Range.

18

For the sills/dykes solutions (SI=1, WS=10), as the window size increases so does the number of solutions (Fig.5.B). Despite showing a similar distribution as in the previous case, their estimations are deeper than in the previous case. North to the North Pyrenean Fault, the solutions display deeper values to the west than to the east, gathered around the higher value RTP anomalies in the zone. Along the Volcanic Field, deep solutions are found

285   in areas without volcanic outcrops. Depth solutions in the western termination of the Ebro Basin, South Pyrenean Zone, Axial Zone and North Pyrenean Zone (From 10 km to more than 20 km) could be related to a deepening of the top of the basement. Values of 10 km are calculated in the border of the Gulf of Lyon offshore RTP great anomaly. On the other hand, the shallowest estimations (0.1 km or less) are found in the center of the RTP anomaly in the Aquitaine Basin, crossed by the Sub-Pyrenean Thrust (Fig.5.B). However, the outcropping materials do not

290   have a relevant magnetic response in the RTP map (Fig.2.B).
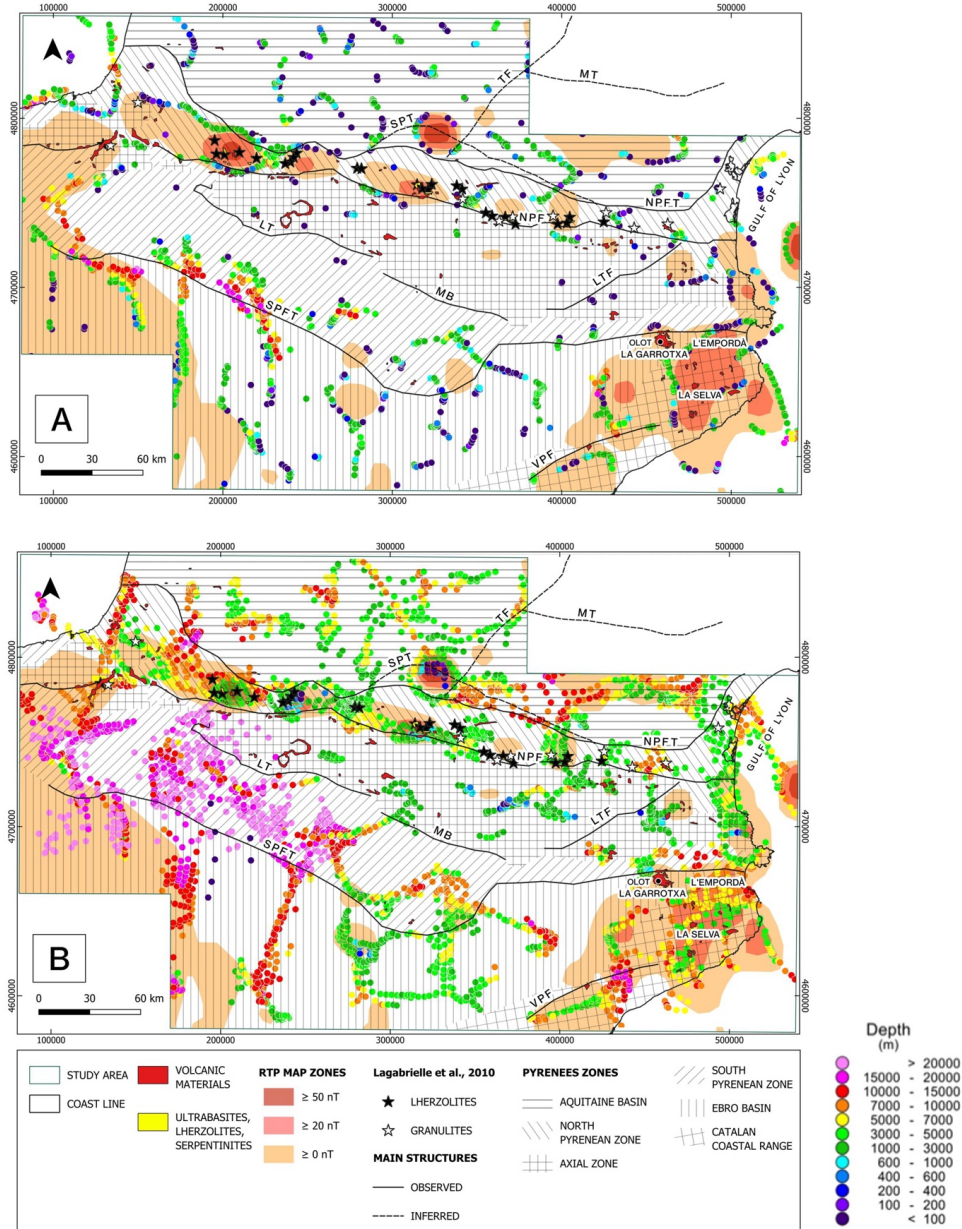
Fig.5. RTP above 0 nT map in addition to (A) Euler solution for SI:0 WS:5; (B) Euler solution for SI:1 WS:10. Main structures and Pyrenean zones differentiated by diverse texture patterns are also represented. MT: Mazamet Thrust, TF: Tolouse Fault, SPT: Sub-Pyrenean Thrust, NPFT: North Pyrenean Frontal Thrust, NPF: North Pyrenean Fault, LTF: La tet Fault, MB: Morreres Back Thrust, LT: Lakora Thrust, SPFT: South Pyrenean Frontal Thrust, VPF: Valles-Penedes Fault. Volcanic materials, lherzolites, Lagabrielle et al., (2009) lherzolite and granulite mapping, Gulf of Lyon, La Selva, L'Empordà, La Garrotxa and Olot are highlighted. UTM coordinates in m, Zone 31N, ETRS89 datum.

295

4.4. Power spectrum.

300

which area analyzed, how large a window, was fractal parameter considered (see Maus and Dimri, 1994 GRL, Ravat et al, 2016, Geosphere)? If fractalness of the field not considered, then the depths are maximum depth estimates from the analysis - needs to be mentioned

This specifically discusses Fig. 6 so refer to it first, tell us about why it was chosen.

Maximum depth to the top are around 21-23 km from this plot.

The radially averaged spectrum cosists mainly in three components. A very steep segment (green) that shows a low wavenumber (0.001-0.016 km^{-1}). The maximum depth displayed for this segment reaches up to 23 km. The next segment (pink) ranges between wavenumbers from 0.016 to 0.084 km^{-1}. This segment displays the shallower sources and noise, reaching up to 15 km. As for the third segment (blue), comprising wavelength values from 0.084 to 0.14 km^{-1} shallower depths are reached, around 12 km. This depth values agree with Andrés et al. (2018) depictions for most of the Curie-Point depths (CDP) in the Pyrenees, pointing to maximum values of 22-24 km depth.

to the top

How are the 2D anomaly trends affecting the radially averaged power spectrum interpretation?

Were many such estimates in different parts calculated?

*** This analysis gives the depth to the top of different magnetic layers and not the depth to the bottom. For the depth to the bottom from centroid estimates, see Tanaka et al. (1999, Tectonophysics) or the de-fractal method (Salem et al., 2014, Tectonophysics; Ravat et al., 2016, Geosphere

***
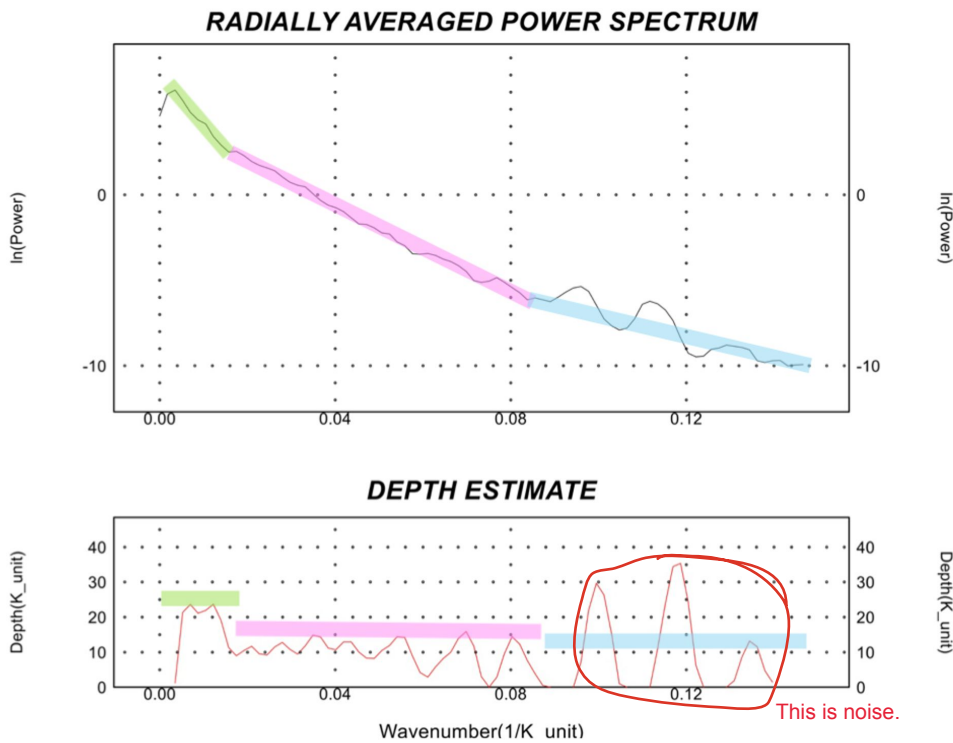
This plot shows instantaneous (short wavenumber segment) estimates and it should be labeled and described as such.

This is noise.

Fig.6. Radially averaged power spectrum of the RTP magnetic field. The wavelength range spans from 7.14 to 125 km. The maximum depth values reach 35 km.

Maximum depth to the top are around 21-23 km from this plot and the slopes of spectra.

5. Discussion.

5.1. Magnetic fabric.

The magnetic texture within the study area is complex and displays a pronounced heterogeneity in terms of source type, distribution and shape. In order to highlight these parameters through the relationship between the magnetic transformations and the geological structures and lithologies, we have built three merged maps displayed on Fig. 7: (1) A ternary image combining the RTP (Fig.3.A) grid, the Analytic Signal (Fig.4.F) grid and the VDR_Z (Fig.4.A) together with the main lineaments of the HDR_X, HDR_Y, HDR_110 and HDR_200 (Fig.4.B, C, D, E) shown on Fig.7.A; (2) The geological map with the RTP anomalies above 0 nT and the gravimetric maximums (Fig.7.B); (3) The TDR (Fig.4.G) with the main structures and the Axial Zone mapping (Fig.7.C).
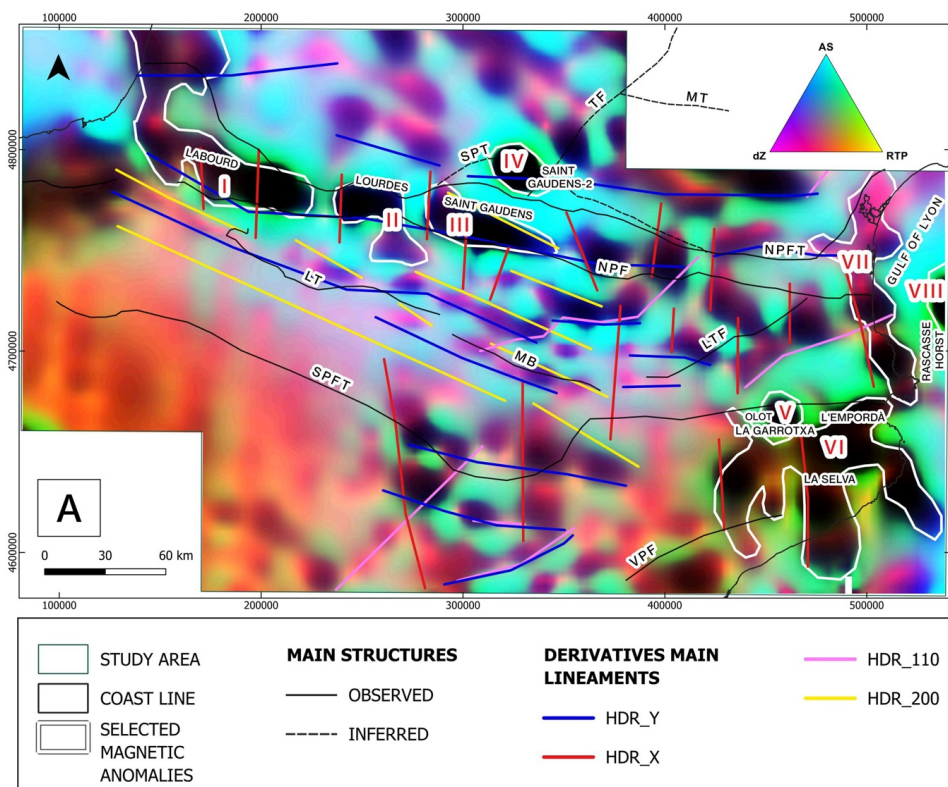
refer to RTP and gravity maps.

to enhance anomalous locations
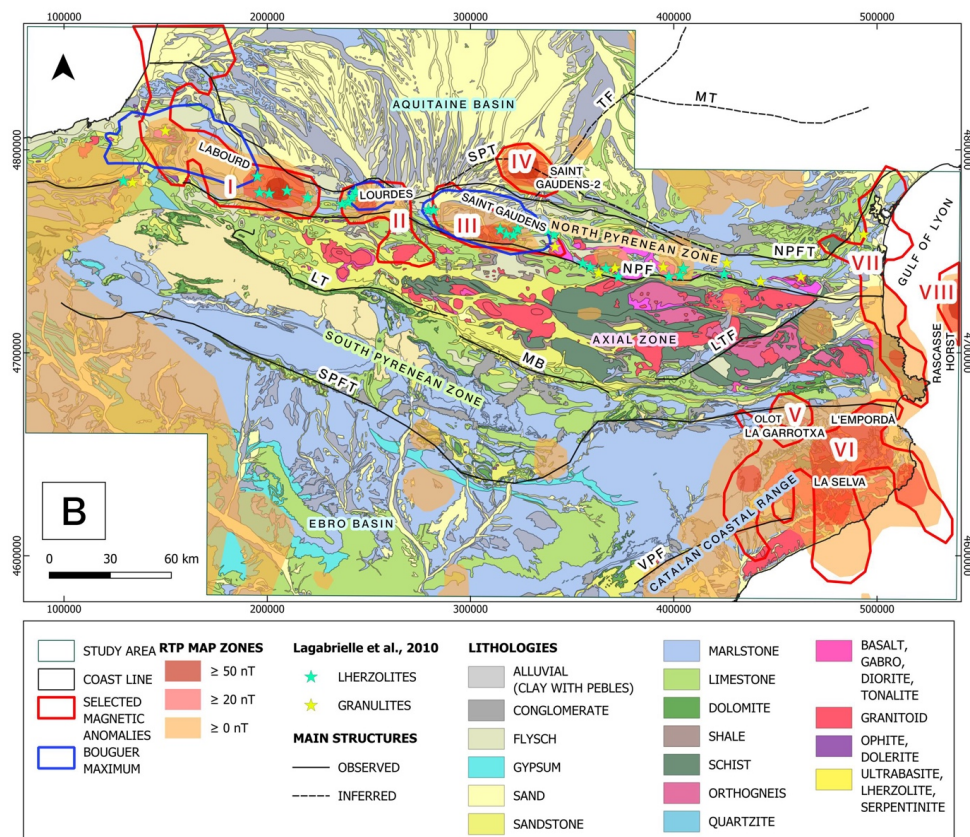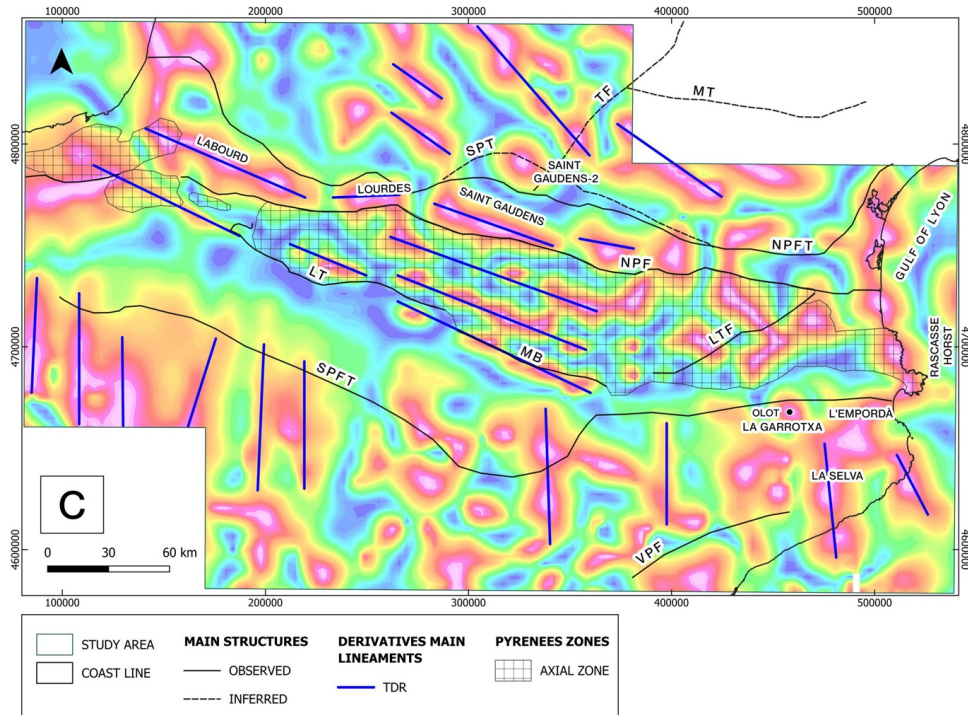
Fig.7. (A) Ternary image (RTP-AS-VDR_Z) together with the horizontal derivatives lineaments mapping (colour lines) and the selected magnetic anomalies (white lines). (B) Lithological map of the study area in addition to the reduced to the magnetic pole above 0 nT mapping, gravimetric maximums (blue lines) and selected magnetic anomalies (red lines). (C) Correlation between the tilt derivative mapping (blue lines) and the main structures (black lines) with the TDR grid as template and the AZ as a pattern mapping. Main structures represented in black lines for the three maps. In blue: LA: Labourd, L: Lourdes, SG: Saint Gaudens. In red: MT: Mazamet Thrust, TF: Tolouse Fault, SPT: Sub-Pyrenean Thrust, NPFT: North Pyrenean Frontal Thrust, NPF: North Pyrenean Fault, LTF: La tet Fault, MB: Morreres Back Thrust, LT: Lakora Thrust, SPFT: South Pyrenean Frontal Thrust, VPF: Valles-Penedes Fault. I: Labourd, II: Lourdes, III: Saint Gaudens, IV: Saint Gaudens-2, V: Olot, VI: L'Emporda-La Selva, VII: East Coast, VIII: Rascasse Horst. UTM coordinates in m, Zone 31N, ETRS89 datum.

The most outstanding anomaly zones have been selected with the following criteria: Firstly, as shown in Figure 7.A, those areas where high and similar values of RTP, Analytic Signal and VDR_Z coincide, hence displayed in black color, are regarded as most certain evidence of subsurface anomalous bodies. However, their shape is more accurately constrained by the TDR_THDR peak values (white lines in Fig.7.A), which nearly matches with the shape of the black zones (Fig.7.A). Then, high RTP values (from 20 nT to 50 nT, reaching 70 nT in zone VIII and near 85 nT in zone IV) and the concurrency with Bouguer anomalies (anomalies I, II, III) (Fig.7.B) were also considered for the selection. These anomalies, labelled as I to VIII in Figures 7. A and B correlate with outcrops of magnetic bodies but also allow delimiting the buried part of these source bodies.

Mapping the main lineations of the horizontal derivatives (X, Y, N200°E and N110°E direction) (Fig.7.A), allows to portrait the magnetic and tectonic fabric. Lineaments with a strong N-S component such as HDR_X and HDR_110 are mostly grouped in the eastern area while those with a predominant E-O component, HDR_Y and HDR_200, are assembled along the Axial Zone and prevail in the western sector. This could imply that the presence of predominantly E-O structures to the west could be linked to the compressive structures related to the

24

350   Pyrenees formation while the predominantly N-S structures could be associated to extensive structures generated
       as consequence of the opening of the northwestern Mediterranean Sea.

       The N-S structures defined by the HDR_X lineaments outline the edges of some anomalies that could be related
       to evaporites to the south-west (Zeyen and Banda, 1989) while the eastern ones seem to be affected by the volcanic
       field of L'Empordà, La Selva and La Garroxa. This N-S lineation may be connected by the volcanic arrangement
       since the most notorious anomalies linked to the volcanic materials appear to the east of the lineation while the

355   western side appears to be less magnetic (Fig.7.A and B). This layout may be related to a fault system setting that
       places shallow bodies to the east of the lineaments, whereas western bodies may be located in structurally deeper
       positions. Additionally, another N-S lineation seems to outline the northwestern edge of the Catalan Coast
       anomaly and could be linked to the intrusion of the magnetic source materials (anomaly VII). Regarding to the
       N110ºE direction lineations (Fig.4.D and 7.A), the southern-central ones appear to constrain the evaporite bodies

360   alongside the HDR_X and HDR_Y lineaments. At both sides of La Tet Fault (LTF), lineations with N110ºE
       direction are mapped (Fig.7.A), which may imply the presence of similar structures along the eastern end of the
       Axial Zone.

       On the other hand, the lineations with a E-O component (HDR_Y and HDR_200) constrain the configuration of
       the Axial Zone. HDR_Y lineations mimic the pathway of the North Pyrenean Fault to the north, as well as the

365   Lakora Thrust and the Morreres Back Thrust to the south. When combined with the HDR_200 lineaments, they
       outline the anomaly of the southern border of the Axial Zone as well as the morphology of the Saint Gaudens
       anomaly (III). To the south, they define a parallel texture which may be related to the presence of evaporites (e.
       g. Santolaria et al., 2020).

       Lastly, the tilt derivative peak mapping exposes the pathway of the structures such the North Pyrenean Frontal

370   Thrust, the Morreres Back Thrust and the Lakora Thrust, which delimit the Axial Zone (Fig.7.C). In addition to
       describing these main structural features, this method portrays structural fabric inside the Axial Zone. A N200ºE
       lineament domain is displayed westward that turns into a N110ºE eastwards, adjacent to the La Tet Fault (Fig.7.A
       and B).

       5.2.   Geological interpretation of the magnetic maps.

375   The correlation between the magnetic response of the most remarkable magnetic anomalies (Fig.8.A and B) and
       their geological context (Fig.2.A) can be interpreted as follows.
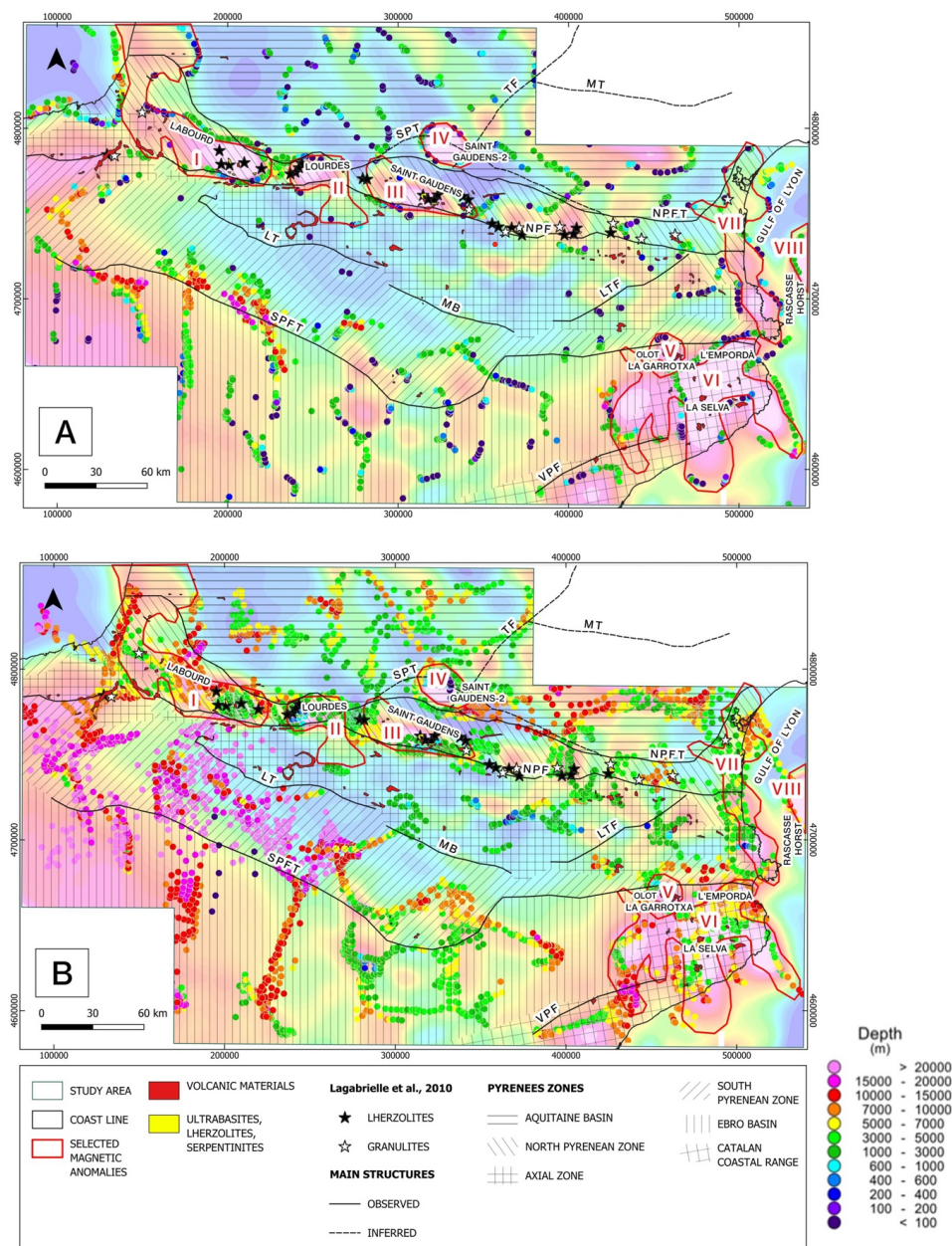
Fig.8. Reduced to the pole magnetic map of the study area with the (A) Euler solution for SI:0 WS:5; (B) Euler solution for SI:1 WS:10 on top. Main structures and Pyrenean zones differentiated by diverse texture patterns are represented. MT: Mazamet Thrust, TF: Tolouse Fault, SPT: Sub-Pyrenean Thrust, NPFT: North Pyrenean Frontal Thrust, NPF: North Pyrenean Fault, LTF: La tet Fault, MB: Morreres Back Thrust, LT: Lakora Thrust, SPFT: South Pyrenean Frontal Thrust, VPF: Valles-Penedes Fault. Volcanic materials, lherzolites, Lagabrielle et al., (2009) lherzolite and granulite mapping are displyed. I: Labourd, II: Lourdes, III: Saint Gaudens, IV: Saint Gaudens-2, V: Olot, VI: L'Emporda-La Selva, VII: East Coast, VIII: Rascasse Horst.

5.2.1. Aquitaine Basin.

26

Located in the southern border of the Aquitaine Basin, the anomaly IV has previously been interpreted by Le Marie et al. (2021) as a slice of sub-continental mantle. Despite the absence of lherzolite or granulite outcrops (Fig.2.B and 7.B) and the mild gravimetric response (Fig.3.B and C), it may correspond to a portion of

390 serpentinized mantle (e.g. Pedrera et al., 2017). Nonetheless, it looks like that this anomaly cuts the trace of the Sub-Pyrenean Thrust (SPT) possibly indicating a late feature. Moreover, it is almost symmetrical circular shape could imply a highly magnetic and low-density vertical dyke-like body as the anomaly source whose intrusion could be linked to the SPT.

In the RTP map, Anomaly IV displays a magnetic response up to + 83 nT, the highest in the study area. According

395 to Euler solutions, it exhibits the shallowest depths for SI=0 (0.1 to3 kilometers) suggesting the presence of a body at those depths (Fig.5.A and 8.A). SI=1 shows a well-shaped circular geometry with average depth up to 7 km (Fig.5.B and 8.B), which are consistent with the depths from Chevrot et al. (2018) and could support the hypothesis of the dike. These solutions coincide with the positive anomaly displayed on the RTP (Fig.3.A and 7.B) to the east and west from the anomaly VI, both indexes present deep solutions (up to 10 km in some places, on SI=1)

400 even though the intensity of the RTP is low.

5.2.2. North Pyrenean Zone.

The presence of mantle material such as granulites, lherzolites and serpentinites at relatively shallow depths (Casas et al., 2019) along the NPZ (Fig.2.C) is interpreted as the source for anomalies I, II and III. The lherzolite and granulite cartography compilation of Lagabrielle et al. (2010) supports this hypothesis since the outcrops overlain

405 the extension of these anomalies (Fig.7.B).

Euler solutions for SI=0 outline the edge of the anomalies while the clusters of SI=1 suggest depths between 0 and 15 km, commonly between 1 and 5 km and reaching more than 20 km for the northwestern areas of anomaly I (Fig.8.A and 8.B).

In addition, trace of anomalies I, II and III match exceptionally well with the outline of the gravimetric anomalies

410 (Fig.7.B), also located between the NPFT and the NPF. The shape of these anomalies displayed in the RTP map (Fig.3.A) is a WNW-ESE oriented elongated shape, however the ternary image (Fig.7.A) suggest a more uneven shape that could reveal the source extension at greater depths.

Regarding the Euler solutions, these anomalies are not well defined for SI=0. For SI=1, the deep solutions are found approximately at the edges of the anomalies (up to 15 km) while shallow depths are registered at the center

415 of the clusters (up to 1 km) (Fig.5.B and 8.B). Anomaly II, for SI=1, displays depths under 1 km for most of its western area, similar to previously reported depths (Biteau et al., 2006) and probably related to the Molasse Neogene. Labourd anomaly (I) appears to be continued towards the NW, probably deepening as depicted in the Euler Solutions (SI=0 and SI=1) (Fig.8.A and B). Lourdes anomaly (II) seems to be connected to a southern small WNW-ESE oriented body that appears to be at an intermediate depth (1 to 3 km) from the Euler solutions (Fig.8.A

420 and B). Saint Gaudens anomaly (III) has an elongated shape that, in the Euler Solutions, is delineated by a string of solutions with depth ranging between 0.6 and 7 km.

5.2.3. Axial Zone.

As shown in Fig.1.A and 3.A, the Axial Zone does not exhibit any remarkable anomalies along the Pyrenees Mountain Range (anomalies range between –20 to 0 nT). The absence of highly magnetic bodies derived from

425 the mantle is consistent with the structural architecture of the Axial Zone, formed by a thick alpine stack of basement thrust sheets. Therefore, in contrast to the North Pyrenean Zone, Axial Zone magnetic mild response

may be on account of an increase of the upper crustal thickness and the fact that the granitoids and other intrusive rocks have very low magnetic susceptibility, most of them falling on the paramagnetic domain (Pueyo et al., 2022) Nevertheless, the anomaly VII, located at the eastern coastline, present values of at least + 20 nT. Its trace follows

430 northward from the main RTP anomaly, as portrayed in the ternary image (Fig.7.B), and represents the transition zone between the Axial Zone, the Mediterranean coast and the westernmost Gulf of Lyon. The outcrops of Cambrian meta-basaltic rocks, as well as Pleistocene volcanic rocks buried which show small outcrops in this area may be the anomaly source.

Zone VII is not well defined in the Euler Solutions. The values of the solutions (Fig.8.A and B) are shallower for

435 SI=0 (up to 5-7 km) and deeper for SI=1 (up to 7-10 km), yet in both cases the source of the anomalies deepen towards the north.

It is significant to highlight the existence of low intensity anomalies that have the same orientation as the LTF to its west (Fig.3.A) as well as the northern area of anomaly V, which reaches depths of 3-5 km, probably indicating the presence of buried volcanic materials (Fig.7.B).

440 **5.2.4. South Pyrenean Zone.**

The RTP map (Fig.1.A and 3.A) reveals a rather low magnetic response for the SPZ. Its south-central area displays values up to 6 nT (Fig.7.B). It is interpreted as the presence of underlying Triassic evaporites and ophites (Zeyen and Banda, 1989). The Euler solutions of SI=0 mainly follow the SPFT with depths that can reach up to 2 km westwards. By contrast, SI=1 describes two distinct areas, a deeper area (7 to 20 km) in the western half and a

445 shallower area (0.2 to 10 km) to the east (Fig.8.A and B).

5.2.5. Catalan Coastal Range.

Characterized by high positive anomalies (20-50 nT) in the RTP map (Fig.1.A and 3.A), the CCR structure is also highlighted by the derivatives (e.g. Fig.4.G) and the ternary image (Fig.7.A). These are linked to the anomalies V and VI on Fig.7.A and B.

450 Anomaly V, located around the town of Olot correspond to the outcrop of basalts and basanites of the La Garrotxa volcanic unit (Zeyen et al., 1991). This Neogene and Quaternary volcanic materials are genetically correlated to those of anomaly VI. The latter compromises the L'Empordà and La Selva volcanic units which are mainly Neogene (Araña et al. 1983, Zeyen et al., 1991). These volcanic terrains that extend offshore involve few volcanic outcrops, however, there is a great amount of granitoids outcropping. The inferred underlaying basalts as well as

455 the granitoids may result in a high range of RTP anomaly values, mainly for the L'Empordà and La Selva terrains, since they display values above 50 nT.

For the Euler solutions, anomaly V seems to display shallow solutions towards the edges for SI = 0 (<0.1 – 0.2 km), reaching 1-5 km for SI=1 (Fig.8.A and B). Anomaly VI values go around 1-5 km for the SI=0 (Fig.8.A) around the edges and from 5-10 km for the buried volcanic materials for SI=1 (Fig.8. B), reaching up to 20 km in

460 the westernmost areas.

5.2.6. Ebro Basin.

The RTP map displays anomaly values above 0 nT with a mainly N-S orientation for most of the area. The Triassic rocks associated to the central anomalies in the South Pyrenean Zone seem to extend southwards, showing the lowest magnetic anomaly values across the area. However, westward within the area, a high anomaly value (+10

465 nT) appears gradually portraying the northern edge of the Iberian Chain (Fig.1.A and 3.A) that could be related to a shallower top of the basement.

5.2.7. Gulf of Lyon.

the

Anomaly VII represents de abrupt eastern end of the Pyrenees Mountain Range as the magnetic fabric changes drastically in the North-Western Mediterranean Sea (Canva, A. et al., 2020). This is suggested to be related to the 470 Oligocene-Miocene rifting that opened the Western Mediterranean Sea with a progressive thinning of the crustal thickness from the Pyrenees to the Mediterranean Sea (Mauffret et al., 2001). The presence of the Catalan Transfer Zone as well as other NW-SE structural lineations, crucial during the opening Gulf of Lyon, (Canva, A. et al., 2020) may be genetically linked to the NW-SE magnetic anomalies, such as VIII.

This anomaly comprises the Rascasse Horst, part of a NE-SW horst-graben display of thinned continental crust 475 (Gorini, 1993; Séranne et al., 1995; Gailler et al., 2009; Moulin et al., 2015; Canva, A. et al., 2020). The absence of volcanic evidence and the presence of a deep Moho, points to a relatively thicker crustal block with mafic intrusions (Canva, A. et al., 2020) as the source for anomaly VIII. The RTP intensity values reaches values up to + 70 nT which represents the second highest anomaly values among the study area (Fig.3.A and 7.B). Anomaly VIII outline displays a homogeneous depth around 1-3 km for Euler solutions of SI=0 (Fig.8.A) as previously 480 described by Canva, A. et al. (2020).

6. Conclusions.

The EMAG2v2 magnetic data transformations for the Pyrenees area have provided new insights into the geological interpretation of the magnetic pattern. The magnetic response for the different domains has portrayed textures that are consistent with the main Pyrenean lineaments. The qualitative interpretation of the magnetic field 485 data has resulted in a comprehensive delineation of eight main distinctive magnetic anomalies. Through Euler

why capitalize?

solutions and Power Spectrum calculations, depth estimations for each zone has been calculated according to the most relevant morphologies, contacts and sills/dykes. The integration of the geological map and the magnetic transformations has shed light on the intricate pattern of structures and materials that comprise the selected anomalies. Furthermore, the utilization of the tilt derivative method has provided a delineation of the borders of 490 the Axial Zone materials, while the combination of the horizontal derivatives lineations have exposed two different structural domains. The absence of more detailed studies such as petrophysical, structural or geophysical surveys bring in some level of uncertainty into the interpretation. Hence, this study is put forward as a groundwork for future researches aimed to define the magnetic fabric and deep structure of the Pyrenees Mountain Range in specific areas that could be of interest, for instance, to investigate its geothermal potential.

495

Data availability

The data used for this study is available for free in different repositories. Magnetic intensity data has been obtained through EMAG website (https://geomag.colorado.edu/emag2-earth-magnetic-anomaly-grid-2-arc-minute-resolution.html). Gravity data for the Pyrenees is available under request and free of charge at IGME (Spanish

link says page not found

500 Geological Survey) repository, from SIGEOF- Geophysical information system (https://info.igme.es/SIGEOF/). Geological and structural maps of the Pyrenees at 1:400.000 can also be obtained for free at IGME repository (http://info.igme.es/cartografiadigital/geologica/mapa.aspx?parent=../tematica/tematicossingulares.aspx&Id=14 &language=es).

https://geomag.colorado.edu/geomagnetic-and-electric-field-models

505 **Author contribution**

- Conceptualization: A. Gamisel-Muzás, R. Soto, C. Ayala.

- Formal analysis: A. Gamisel-Muzás, R. Soto, C. Ayala, T. Mochales, F. M. Rubio, P. Clariana.

- Founding acquisition: R. Soto, C. Ayala.

510

- Investigation: A. Gamisel-Muzás, R. Soto, C. Ayala, T. Mochales, F. M. Rubio, P. Clariana, C. Rey-Moral.

- Methodology: : A. Gamisel-Muzás, R. Soto, C. Ayala, T. Mochales, , C. Rey-Moral, J. Martín-León.

- Project Administration: R. Soto, C. Ayala.

- Software: A. Gamisel-Muzás, C. Ayala, T. Mochales, C. Rey-Moral, J. Martín-León.

- Resources: A. Gamisel-Muzás, C. Ayala, J. Martín-León.

515

- Supervision: R. Soto, C. Ayala, T. Mochales

- Writing of the original draft: A. Gamisel-Muzás, R. Soto, P. Clariana.

- Writing review and editing: A. Gamisel-Muzás, R. Soto, C. Ayala, T. Mochales, F. M. Rubio, P. Clariana, C. Rey-Moral, J. Martín-León.

520 **Competing interest**

The authors declare that they have no conflict of interest.

Acknowledgements

References

Alibert, C. (1985). A Sr-Nd isotope and REE study of Late Triassic dolerites from the Pyrenees (France) and the Messejana Dyke (Spain and Portugal). Earth and Planetary Science Letters, 73(1), 81-90.

535 Alonso-Zarza, A. M., Armenteros, I., Braga, J. C., Muñoz, A., Pujalte, V., Ramos, E., ... & Villena, J. (2002). Tertiary.

Andrés, J., Marzán, I., Ayarza, P., Martí, D., Palomeras, I., Torné, M., ... & Carbonell, R. (2018). Curie point depth of the Iberian Peninsula and surrounding margins. A thermal and tectonic perspective of its evolution. Journal of Geophysical Research: Solid Earth, 123(3), 2049-2068.

540 Ansari, A. H., & Alamdar, K. (2009). Reduction to the pole of magnetic anomalies using analytic signal. World Applied Sciences Journal, 7(4), 405-409.

Araña, V., Aparicio, A., Martín Escorza, C., Garcia Cacho, L., Ortiz, R., Vaquer Navarro, R., ... & Gassiot, X. (1983). El volcanismo neógeno-cuaternario de Catalunya: caracteres estructurales, petrológicos y geodinámicos.

Ayala, C., Kimbell, G. S., Brown, D., Ayarza, P., & Menshikov, Y. P. (2000). Magnetic evidence for the geometry

545 and evolution of the eastern margin of the East European Craton in the Southern Urals. Tectonophysics, 320(1), 31-44.

Baranov, V. (1957). A new method for interpretation of aeromagnetic maps: pseudo-gravimetric anomalies. Geophysics, 22(2), 359-382.

Baranov, V., & Naudy, H. (1964). Numerical calculation of the formula of reduction to the magnetic pole. Geophysics, 29(1), 67-79.

Barnolas, A., Chiron, J. C., Guérangé, B. (1996).Synthese géologique et géophysique des Pyrénées: introduction, Géophysique, Cycle hercynien. Bureau de Recherches Géologiques et Minières, 1996.

Barnolas, A. & Pujalte, V. (2004). La Cordillera Pirenaica: Definición, límites y división.

Beaumont, C., Muñoz, J. A., Hamilton, J., & Fullsack, P. (2000). Factors controlling the Alpine evolution of the central Pyrenees inferred from a comparison of observations and geodynamical models. Journal of Geophysical Research: Solid Earth, 105(B4), 8121-8145.

Beziat, D. (1983). Etude pétrologique et géochimique des ophites des Pyrenees. Implications géodynamiques [These de 3 cycle] Universite de Toulouse.

Biteau, J. J., Le Marrec, A., Le Vot, M., & Masset, J. M. (2006). The aquitaine basin. Petroleum Geoscience, 12(3), 247-273.

Blakely, R. J., Connard, G. G., & Curto, J. B. (2016). Tilt derivative made easy. Geosoft Technical Publications, 4, 1-4.

Bond, R. M. G., and K. R. McClay. "Inversion of a Lower Cretaceous extensional basin, south central Pyrenees, Spain." Geological Society, London, Special Publications 88.1 (1995): 415- 431.

Cámara, P., & Klimowitz, J. (1985). Interpretación geodinámica de la vertiente centro-occidental surpirenaica (Cuencas de Jaca-Tremp). Estudios geológicos, 41(5-6), 391-404.

Campanyà, J., Ledo, J., Queralt, P., Marcuello, A., Liesa, M., & Muñoz, J. A. (2011). Lithospheric characterization of the Central Pyrenees based on new magnetotelluric data. Terra Nova, 23(3), 213-219.

Canérot, J., Hudec, M. R., & Rockenbauch, K. (2005). Mesozoic diapirism in the Pyrenean orogen: Salt tectonics on a transform plate boundary. AAPG bulletin, 89(2), 211-229.

Canva, A., Thinon, I., Peyrefitte, A., Couëffé, R., Maillard, A., Jolivet, L., ... & Guennoc, P. (2020). The Catalan magnetic anomaly: Its significance for the crustal structure of the Gulf of Lion passive margin and relationship to the Catalan transfer zone. Marine and Petroleum Geology, 113, 104174.

Casas, J. M., Álvaro, J. J., Clausen, S., Padel, M., Puddu, C., Sanz-López, J., ... & Sanz-López, J. (2019). Palaeozoic basement of the Pyrenees. In The Geology of Iberia: A Geodynamic Approach: Volume 2: The Variscan Cycle (pp. 229-259). Cham: Springer International Publishing.

Casas, A., Kearey, P., Rivero, L., & Adam, C. R. (1997). Gravity anomaly map of the Pyrenean region and a comparison of the deep geological structure of the western and eastern Pyrenees. Earth and Planetary Science Letters, 150(1-2), 65-78.

Chevrot, S., Sylvander, M., Diaz, J., Martin, R., Mouthereau, F., Manatschal, G., ... & Ruiz, M. (2018). The non-cylindrical crustal architecture of the Pyrenees. Scientific reports, 8(1), 9591.

Chevrot, S., Villaseñor, A., Sylvander, M., Benahmed, S., Beucler, E., Cougoulat, G., ... & Wolyniec, D. (2014). High-resolution imaging of the Pyrenees and Massif Central from the data of the PYROPE and IBERARRAY portable array deployments. Journal of Geophysical Research: Solid Earth, 119(8), 6399-6420.

Choukroune, P. (1989). The ECORS Pyrenean deep seismic profile reflection data and the overall structure of an orogenic belt. Tectonics, 8(1), 23-39.

https://doi.org/10.5194/egusphere-2024-1602
Preprint. Discussion started: 6 June 2024
© Author(s) 2024. CC BY 4.0 License.

Clerc, C., & Lagabrielle, Y. (2014). Thermal control on the modes of crustal thinning leading to mantle exhumation: Insights from the Cretaceous Pyrenean hot paleomargins. Tectonics, 33(7), 1340-1359.

Clerc, C., Lagabrielle, Y., Neumaier, M., Reynaud, J. Y., & de Saint Blanquat, M. (2012). Exhumation of subcontinental mantle rocks: evidence from ultramafic-bearing clastic deposits nearby the Lherz peridotite body, French Pyrenees. Bulletin de la Société géologique de France, 183(5), 443-459.

Cooper, G. R. J. (2008). Euler deconvolution with improved accuracy and multiple different structural indices. Journal of china university of Geosciences, 19(1), 72-76.

Deramond, J., P. Baby, M. Specht, and G. Crouzet (1988), Geometrie des chevauchements dans laZone nord-pyreneenne ariegeoise precisee par leprofil ECORS,Bull. Soc. Geol. Fr.,6(2), 287–294.

Fanton, G., Martínez, P., & Giménez, M. (2014). Procesamiento y analisis cualitativo de datos aeromagneticos con vistas a la exploración de yacimientos hidrotermales tipo lode gold-provincia de La rioja, Argentina. Geoacta, 39(1), 30-50.

FitzGerald, D., Milligan, P., & Reid, A. (2004). Integrating Euler solutions into 3D geological models-automated mapping of depth to magnetic basement. In SEG Technical Program Expanded Abstracts 2004 (pp. 738-741). Society of Exploration Geophysicists.

Ford, M., Masini, E., Vergés, J., Pik, R., Ternois, S., Léger, J., ... & Calassou, S. (2022). Evolution of a low convergence collisional orogen: a review of Pyrenean orogenesis. Bulletin de la Société Géologique de France, 193(1).

Gailler, A., Klingelhoefer, F., Olivet, J. L., Aslanian, D., & Technical, O. B. S. (2009). Crustal structure of a young margin pair: New results across the Liguro–Provencal Basin from wide-angle seismic tomography. Earth and Planetary Science Letters, 286(1-2), 333-345.

García-Lobón, J. L., & Ayala, C. (2007). Cartografía geofisica de la República Dominicana: Datos de densidad, susceptibilidad magnética y magnetización remanente. La Geología de la República Dominicana. Boletín Geológico y Minero, 118(2), 157-174.

García-Sansegundo, J. (1996). Hercynian structure of the Axial Zone of the Pyrenees: the Aran Valley cross-section (Spain-France). Journal of Structural Geology, 18(11), 1315-1325.

García-Sansegundo, J., Poblet, J., Alonso, J. L., & Clariana, P. (2011). Hinterland-foreland zonation of the Variscan orogen in the Central Pyrenees: comparison with the northern part of the Iberian Variscan Massif. Geological Society, London, Special Publications, 349(1), 169-184.

Garrido Megías, A. (1973). Estudio geologico y relación entre tectónica y sedimentación del Secundario y Terciario de la vertiente meridional pirenaica de la zona central (Huesca y Lérida). Teisis doctoral. Universidad de Granada, 395 pp.

Gibson, R. I., & Millegan, P. S. (Eds.). (1998). Geologic applications of gravity and magnetics: Case histories. Society of Exploration Geophysicists and American Association of Petroleum Geologists.

Golynsky, A. V., Alyavdin, S. V., Masolov, V. N., Tscherinov, A. S., & Volnukhin, V. S. (2002). The composite magnetic anomaly map of the East Antarctic. Tectonophysics, 347(1-3), 109-120.

Gorini, C., Mauffret, A., Guennoc, P., & Le Marrec, A. (1994). Structure of the Gulf of Lions (northwestern Mediterranean Sea): A review. Hydrocarbon and petroleum geology of France, 223-243.

625   Hayatudeen, M., Rasaq, B., Onaolapo, R. I., & Abe, A. O. (2021). First horizontal and first vertical derivatives
        from high resolution aeromagnetic data over the Gongola basin upper Benue trough Northeastern Nigeria. Global
        journal of pure and applied sciences, 27(2), 181-192.

        Jammes, S., Lavier, L., & Manatschal, G. (2010). Extreme crustal thinning in the Bay of Biscay and the Western
        Pyrenees: From observations to modeling. Geochemistry, Geophysics, Geosystems, 11(10).

630   Jammes, S., Manatschal, G., Lavier, L., & Masini, E. (2009). Tectonosedimentary evolution related to extreme
        crustal thinning ahead of a propagating ocean: Example of the western Pyrenees. Tectonics, 28(4).

        Lagabrielle, Y., Labaume, P., & de Saint Blanquat, M. (2010). Mantle exhumation, crustal denudation, and gravity
        tectonics during Cretaceous rifting in the Pyrenean realm (SW Europe): Insights from the geological setting of
        the lherzolite bodies. Tectonics, 29(4).

635   Lahti, I., & Karinen, T. (2010). Tilt derivative multiscale edges of magnetic data. The Leading Edge, 29(1), 24-
        29.

        Langel, R. A., & Hinze, W. J. (1998). The magnetic field of the Earth's lithosphere: The satellite perspective.
        Cambridge University Press.

        Ledo, J., Ayala, C., Pous, J., Queralt, P., Marcuello, A., & Muñoz, J. A. (2000). New geophysical constraints on
640   the deep structure of the Pyrenees. Geophysical research letters, 27(7), 1037- 1040.

        Le Maire, P., Thinon, I., Tugend, J., Issautier, B., Martelet, G., Paquet, F., ... & Canva, A. (2021). New Magnetic
        compilation and interpretation of the Bay of Biscay and surrounding continental shelves. BSGF-Earth Sciences
        Bulletin, 192(1), 58.

        Ma, G., & Li, L. (2012). Edge detection in potential fields with the normalized total horizontal derivative.
645   Computers & Geosciences, 41, 83-87.

        Mauffret, A., de Grossouvre, B. D., Dos Reis, A. T., Gorini, C., & Nercessian, A. (2001). Structural geometry in
        the eastern Pyrenees and western Gulf of Lion (Western Mediterranean). Journal of Structural Geology, 23(11),
        1701-1726.

        Maus, S., Barckhausen, U., Berkenbosch, H., Bournas, N., Brozena, J., Childers, V., ... & Caratori Tontini, F.
650   (2009). EMAG2: A 2–arc min resolution Earth Magnetic Anomaly Grid compiled from satellite, airborne, and
        marine magnetic measurements. Geochemistry, Geophysics, Geosystems, 10(8).

        Maus, S., & Dimri, V. (1995). Potential field power spectrum inversion for scaling geology. Journal of
        Geophysical Research: solid earth, 100(B7), 12605-12616.

        Meyer, B., Chulliat, A., & Saltus, R. (2017). Derivation and error analysis of the earth magnetic anomaly grid at
655   2 arc min resolution version 3 (EMAG2v3). Geochemistry, Geophysics, Geosystems, 18(12), 4522-4537.

        Miller, H. G., & Singh, V. (1994). Potential field tilt—a new concept for location of potential field sources. Journal
        of applied Geophysics, 32(2-3), 213-217.

        Moulin, M., Klingelhoefer, F., Afilhado, A., Aslanian, D., Schnurle, P., Nouze, H., ... & Feld, A. (2015). Deep
        crustal structure across a young passive margin from wide-angle and reflection seismic data (The SARDINIA
660   Experiment)–I. Gulf of Lion's margin. Bulletin de la Société géologique de France, 186(4-5), 309-330.

        Müller, R. D., Sdrolias, M., Gaina, C., & Roest, W. R. (2008). Age, spreading rates, and spreading asymmetry of
        the world's ocean crust. Geochemistry, Geophysics, Geosystems, 9(4).

        Muñoz, J. A. (1992). Evolution of a continental collision belt: ECORS-Pyrenees crustal balanced cross-section.
        Thrust tectonics, 235-246.

665   Muñoz, J. A. (2019). Alpine orogeny: Deformation and structure in the northern Iberian margin (Pyrenees sl). The Geology of Iberia: A Geodynamic Approach: Volume 3: The Alpine Cycle, 433-451.

Nabighian, M. N., Grauch, V. J. S., Hansen, R. O., LaFehr, T. R., Li, Y., Peirce, J. W., ... & Ruder, M. E. (2005). The historical development of the magnetic method in exploration. Geophysics, 70(6), 33ND-61ND.

Pedrera, A., García-Senz, J., Ayala, C., Ruiz-Constán, A., Rodríguez-Fernández, L. R., Robador, A., & González

670   Menéndez, L. (2017). Reconstruction of the exhumed mantle across the North Iberian Margin by crustal-scale 3-D gravity inversion and geological cross section. Tectonics, 36(12), 3155-3177.

Peredo, C. R., Yutsis, V., Martin, A. J., & Aranda-Gómez, J. J. (2021). Crustal structure and Curie point depth in central Mexico inferred from the spectral analysis and forward modeling of potential field data. Journal of South American Earth Sciences, 112, 103565.

675   Poblet, J. (1991). "Estructura herciniana i alpina del vessant sud de la zona axial del Pirineu central." Barcelona, Departament of Geology, Barcelona University (1991).

Pueyo, E. L., Román-Berdiel, T., Calvín, P., Bouchez, J. L., Beamud, E., Ayala, C., ... & García-Lobón, J. L. (2022). Petrophysical Characterization of Non-Magnetic Granites; Density and Magnetic Susceptibility Relationships. Geosciences, 12(6), 240.

680   Purucker, M., & Whaler, K. (2007). Crustal magnetism. Treatise on geophysics, 5, 195-237.

Reid, A. B., Allsop, J. M., Granser, H., Millett, A. T., & Somerton, I. W. (1990). Magnetic interpretation in three dimensions using Euler deconvolution. Geophysics, 55(1), 80-91.

Roest, W. R., & Srivastava, S. P. (1991). Kinematics of the plate boundaries between Eurasia, Iberia, and Africa in the North Atlantic from the Late Cretaceous to the present. Geology, 19(6), 613-616.

685   Rosenbaum, G., Lister, G. S., & Duboz, C. (2002). Relative motions of Africa, Iberia and Europe during Alpine orogeny. Tectonophysics, 359(1-2), 117-129.

Rougier, G., Ford, M., Christophoul, F., & Bader, A. G. (2016). Stratigraphic and tectonic studies in the central Aquitaine Basin, northern Pyrenees: Constraints on the subsidence and deformation history of a retro-foreland basin. Comptes Rendus Geoscience, 348(3-4), 224-235.

690   Saspiturry, N., Allanic, C., Razin, P., Issautier, B., Baudin, T., Lasseur, E., ... & Leleu, S. (2020). Closure of a hyperextended system in an orogenic lithospheric pop-up, Western Pyrenees: The role of mantle buttressing and rift structural inheritance. Terra Nova, 32(4), 253-260.

Socías, I., Mezcua, J., Lynam, J., & Del Potro, R. (1991). Interpretation of an aeromagnetic survey of the Spanish mainland. Earth and planetary science letters, 105(1-3), 55-64.

695   Seguret, M. (1972). Étude tectonique des nappes et séries décollées de la partie centrale du versant sud des Pyrénées. Pub. Estela, Ser geol. struct., 2, 1-155.

Séranne, M., Benedicto, A., Labaum, P., Truffert, C., & Pascal, G. (1995). Structural style and evolution of the Gulf of Lion Oligo-Miocene rifting: role of the Pyrenean orogeny. Marine and Petroleum geology, 12(8), 809-820.

700   Serrano, O., et al. (2006) "Le bassin d'Aquitaine: Valorisation des données sismiques, cartographie structurale et potentiel pétrolier, Rapport Régional d'Evaluation Pétrolière." Bureau de la Recherche Géologique et Minière, Orléans, France 245 (2006).

Soto, R., Casas, A. M., Storti, F., & Faccenna, C. (2002). Role of lateral thickness variations on the development of oblique structures at the Western end of the South Pyrenean Central Unit. Tectonophysics, 350(3), 215-235.

705   Soto, R., Storti, F., & Casas-Sainz, A. M. (2006). Impact of backstop thickness lateral variations on the tectonic architecture of orogens: Insights from sandbox analogue modeling and application to the Pyrenees. Tectonics, 25(2).

Souquet, P., Peybernes, B., Bilotte, M., & Debroas, E. J. (1977). La chaîne alpine des Pyrénées. Géologie alpine, 53(2), 193-216.

710   Spector, A., & Grant, F. S. (1970). Statistical models for interpreting aeromagnetic data. Geophysics, 35(2), 293-302.

Thompson, D. T., 1982, EULDPH-A new technique for making computer-assisted depth estimates from magnetic data: Geophysics, 47, 31-37.

Vauchez, A., Tommasi, A., & Mainprice, D. (2012). Faults (shear zones) in the Earth's mantle. Tectonophysics, 558, 1-27.

715   Verduzco, B., Fairhead, J. D., Green, C. M., & MacKenzie, C. (2004). New insights into magnetic derivatives for structural mapping. The leading edge, 23(2), 116-119.

Vine, F. J. (1966). Spreading of the Ocean Floor: New Evidence: Magnetic anomalies may record histories of the ocean basins and Earth's magnetic field for 2×10^8 years. Science, 154(3755), 1405- 1415.

720   Vine, F. J., & Matthews, D. H. (1963). Magnetic anomalies over oceanic ridges. Nature, 199, 947- 949.

Wang, Y., Chevrot, S., Monteiller, V., Komatitsch, D., Mouthereau, F., Manatschal, G., ... & Martin, R. (2016). The deep roots of the western Pyrenees revealed by full waveform inversion of teleseismic P waves. Geology, 44(6), 475-478.

Wehr, H., Chevrot, S., Courrioux, G., & Guillen, A. (2018). A three-dimensional model of the Pyrenees and their
725   foreland basins from geological and gravimetric data. Tectonophysics, 734, 16-32.

Zeyen, H. J., & Banda, E. (1988). Cartografía geofísica en Cataluña. 1: El mapa aeromagnético. Revista de la Sociedad Geológica de España, 1(1), 73-79.

Zeyen, H. J., & Banda, E. (1989). 2 1/2 and 3 dimensional interpretation of magnetic anomalies in the central-southern Pyrenees (Spain). Geodinamica Acta, 3(3), 229-236.

730   Zeyen, H. J., Banda, E., & Klingelé, E. (1991). Interpretation of magnetic anomalies in the volcanic area of northeastern Spain. Tectonophysics, 192(1-2), 201-210.

Ziegler, P. A. (1988). Evolution of the Arctic-North Atlantic and the western Tethys.

Zwart, H. J. (1986). The Variscan geology of the Pyrenees. Tectonophysics, 129(1-4), 9-27.